https://doi.org/10.5194/egusphere-2026-4780
Preprint. Discussion started: 19 August 2026

Observed and projected changes in extreme precipitation intensity and temporal patterns: a case study of the Misa River Basin (Central Italy)

Dawit Y. Meskele*[1], Antonio Parodi[2], Anna Napoli[4,5], Gianluca Loffredo[3], Maurizio Brocchini[1]

[1]University of Polytechnic Marche, Department of Construction, Civil Engineering, and Architecture (DICEA), Via Brecce Bianche 12, 60131 Ancona, Italy
[2]CIMA Research Foundation, Via Armando Magliotto 17100, Savona, Italy
[3] Presidency of the Council of Ministers, Extraordinary Deputy Commissioner of the Government for the Emilia-Romagna, Marche, and Tuscany 2023 floods, Italy
[4] C3A - Center Agriculture Food Environment, Via Mach 1, San Michele all'Adige, Italy
[5] DICAM - Department of Civil, Environmental and Mechanical Engineering, University of Trento, Via Mesiano 77, Trento, Italy
**Correspondence to* : Dawit Y. Meskele (d.y.meskele@pm.univpm.it)

Abstract

Extreme hydrological events such as floods are intensifying under climate change, yet uncertainties in local-scale rainfall projections impede reliable adaptation strategies. This study examines future rainfall extremes and their daily timing in the Misa River basin (Central Italy) using the Weather Research and Forecasting (WRF) and Consortium for Small-scale Modeling in Climate Mode (COSMO-CLM) models, together with rain gauge observations, comparing historical periods (1979–2008 and 1981–2008, respectively) with a future period (2039–2068) under RCP8.5. Mean-state precipitation is projected to decrease annually and in summer, while November average daily precipitation increases. In contrast, extreme precipitation shows a different pattern: both models project more frequent extremes relative to their own historical baselines, with a historical 100-year event becoming 10–20 times more frequent by mid-century. However, the models diverge when evaluated against observed historical flood events: WRF shows a broadly uniform response, with return periods for past events reduced by nearly 50% while COSMO shows an event-dependent response, with events remaining within the 95% confidence bound. Sub-daily event magnitudes, including average peak intensity and nine-hour maximum accumulation, decrease in both models. Overall, both models agree that extremes intensify in a model-relative sense, but this agreement breaks down against observed benchmarks and sub-daily magnitudes, reflecting model-chain spread rather than uniform intensification. These results suggest that historically based design standards may underestimate future rainfall hazards under some projections, underscoring the need to account for model-chain uncertainty in flood risk planning across the Misa River basin.

Key terms: Climate change projection, convection-permitting models, extreme rainfall, Misa River basin

https://doi.org/10.5194/egusphere-2026-4780
Preprint. Discussion started: 19 August 2026

1. INTRODUCTION

Climate change is increasingly affecting social and ecological systems, impacting human life, endangering security, and influencing numerous industries at various scales worldwide (Aguiar et al., 2018; IPCC, 2023). Although mitigation actions are essential for counteracting global warming by gradually reducing greenhouse gas emissions, there is an immediate need for adaptation to intensifying climate impacts (Ledda et al., 2020). Observational data show that climate change increases the frequency and intensity of extreme events, including heavy rainfall (IPCC, 2023). This aligns with the Clausius-Clapeyron relationship, which indicates that the atmosphere can hold approximately 7% more water vapor per 1°C of warming, thereby increasing the potential for more intense precipitation when dynamical conditions are favorable (Trenberth et al., 2003; Held and Soden, 2006). Moreover, the rate of increase in precipitation extremes is influenced by multiple factors, including changes in the vertical velocity profile, alterations in precipitation efficiency (Hagos et al., 2021; Li et al., 2023) and both direct and indirect soil moisture-precipitation feedback (Manabe and Wetherald, 1987; Findell and Elfatih, 2003).

The Mediterranean region is particularly vulnerable to these changes, where interactions between large-scale atmospheric circulation and complex local topography, especially the Apennine Mountains, strongly shape precipitation patterns (Tartaglione, 2025). Although Regional Climate Models (RCMs) use dynamic downscaling from Global Climate Models (GCMs), they struggle to accurately capture sub-daily convective storms in complex topographic settings (Berg et al., 2019). Convection-permitting models (CPMs), operating at horizontal grid spacing finer than 4 km, explicitly represent deep convective processes, enabling more realistic simulation of short-duration extreme rainfall intensity, frequency, and trends at the basin scale (Pieri et al., 2015; Kendon et al., 2021; Napoli et al., 2023). By directly resolving convective processes, CPMs bridge the gap between regional climate signals and local hydrological impacts, providing the physical detail necessary to ground adaptation strategies in the realities of a warming Mediterranean climate (Kendon et al., 2012; Lucas-Picher et al., 2021).

The Misa River basin in central Italy is a critical case study for extreme rainfall analysis due to its high hydro-meteorological vulnerability and complex drainage configuration. Stretching from the Apennine Mountains to the Adriatic Sea, the basin features steep orographic gradients that have historically driven repeated flooding (Brocchini et al., 2017; Tartaglione, 2025). Forced lifting of

https://doi.org/10.5194/egusphere-2026-4780
Preprint. Discussion started: 19 August 2026

moist Adriatic air over steep slopes produces very short lags between peak rainfall and peak river discharge, making the basin particularly susceptible to flash flooding, resulting in a hazard expected to intensify under climate change. Despite advances in CPM, significant gaps remain at the catchment scale. First, although CPM simulations have been produced for broader Mediterranean and Italian regional domains (Torma et al., 2015; Berthou et al., 2020; Pichelli et al., 2021), their focused application to small, high-vulnerability catchments such as the Misa River basin remains limited, evaluating the RCMs in basin-scale flood risk management (Fosser et al., 2015). Second, existing studies assess generalized return-period statistics, and the distribution of rainfall within an event may shift under future conditions (Westra et al., 2014; Prein et al., 2017; Ban et al., 2020). Third, the recurrence intervals of specific historically catastrophic events have seldom been evaluated under future climate scenarios at the basin and station levels, despite their direct relevance for infrastructure design and civil protection planning (Rajczak and Schär, 2017; Myhre et al., 2019).

To address these gaps and to provide a new methodological framework for the study of the hydrological processes in medium-sized Mediterranean catchments under climate change phenomena, this study combines rain gauge observations with two CPM climate simulations to investigate future changes in extreme rainfall in the Misa River basin under RCP8.5 scenarios. Specifically, this study aims to (1) assess changes in annual-to-seasonal precipitation, extreme rainfall intensity, and change in event frequency between the historical period (1979/81–2008) and the future period (2039–2068); (2) quantify how return periods of specific historically catastrophic flood events will change under future climate conditions at the basin and station levels; (3) characterize shifts in the intra-storm temporal structure of future extreme events using Huff curve analysis; and (4) provide insights applicable to rainfall hazard for infrastructure planning in small Mediterranean catchments.

https://doi.org/10.5194/egusphere-2026-4780
Preprint. Discussion started: 19 August 2026

2. DATA AND METHODS

2.1 Study Area: Misa River Basin

The Misa River basin conveys its flow through Senigallia to the Adriatic Sea, traversing a coastal setting. The basin covers an area of 384 km^2 and the main streamlines stretch roughly 48 km from the Apennine Mountains to the Adriatic Sea. The basin exhibits significant elevation variation, ranging from sea level at the outlet to about 828 m in the upstream mountainous regions (Fig. 1). This pronounced gradient creates a distinct transition from inland hilly terrain to a narrow coastal plain, where the final reach of the river extends for about 10km through an urbanized area (Marco et al., 2021). Hydrologically, the basin stream is organized into branches, with the Nevola stream as the principal tributary and Misa as the mainstream, both originating in the Apennine Mountains, which join the Misa upstream of Senigallia. Land use is predominantly agricultural across most of the basin, with intensive cultivation shaping the runoff process. In contrast, urban development becomes dominant near the outlet, where human interventions, particularly channel construction for infrastructure and settlement, have significantly altered river morphology and reduced flow conveyance capacity (Verol et al., 2020).

Record-breaking rainfall over very short durations has recently intensified extreme events in the basin. For instance, on September 15th, 2022, the surrounding area experienced intense flooding, with cumulative rainfall exceeding 420 mm in just a few hours (Donnini et al., 2023), and the Misa-Nevola basin received over 200 mm. These extreme inputs frequently trigger overbank flow in the river, leading to widespread flooding in adjacent low-lying and urbanized areas. This flood resulted in an estimated damage of approximately 2 billion euros and caused 13 fatalities; the rainfall event mainly affected the border group Northern Marche area, with impacts specifically attributable to the Misa-Nevola area (Corti et al., 2024). A similar event occurred in May 2014: the principal flooding in Senigallia city was associated with the overflow of the Misa River (Mattavelli, 2023), which was associated with intense precipitation driven by a cyclone originating over the Gulf of Genoa (Tartaglione, 2025), resulting in 3 fatalities and damage totaling 180 million euros (Corti et al., 2024). These events are typically associated with the interaction of moisture-laden cyclonic systems and orographic uplift over the Apennines, which intensify and prolong rainfall extremes. The combination of geomorphological constraints, land-use pressures,

https://doi.org/10.5194/egusphere-2026-4780
Preprint. Discussion started: 19 August 2026

and increasingly intense precipitation patterns make the Misa River basin particularly susceptible to flash flooding.

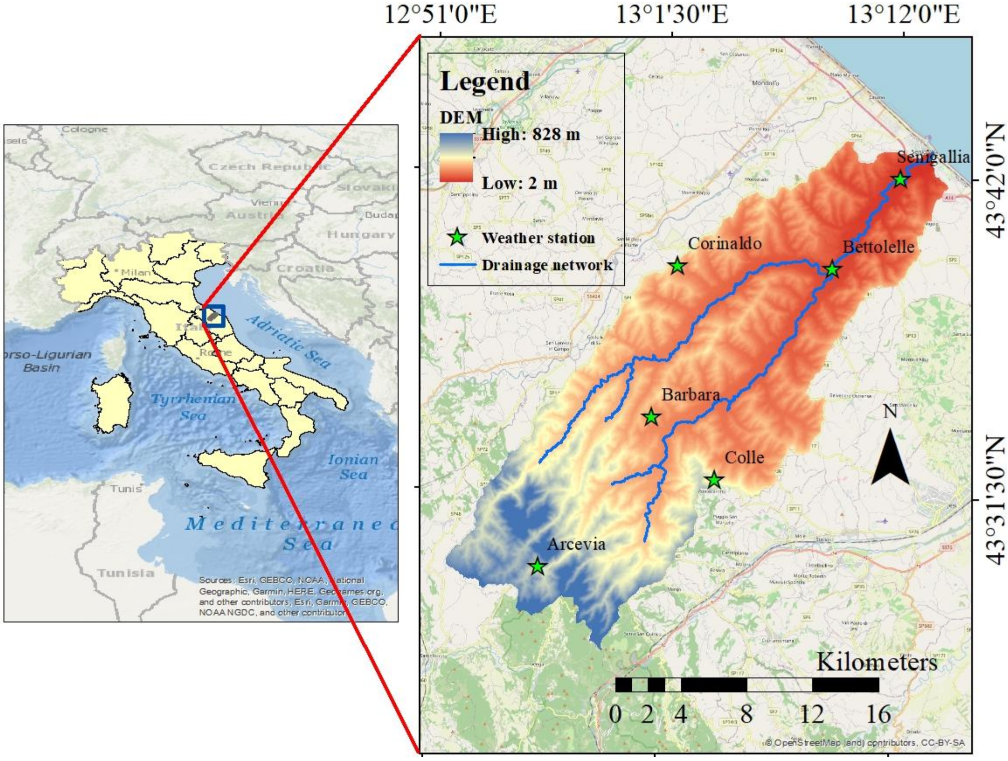

Figure 1. Study area map: Italy with its administrative boundaries (left side) and the Misa River basin, which includes DEM (Digital Elevation Model), weather gauging stations, and the drainage network (right side). Background mapping features of the Misa River basin are derived from OpenStreetMap (data available under the Open Database License, © OpenStreetMap contributors) and the Italian boundary of the Esri Ocean Basemap (Sources: Esri, GEBCO, NOAA, National Geographic, Garmin, and contributors | Powered by Esri).

2.2 Data

This study employs one daily observed precipitation record from 1951 to 2023 and three convection-permitting modeling (CPM) approaches: (1) the Consortium for Small-scale Modelling in Climate Mode (COSMO-CLM), which dynamically downscales the CMIP5 global model CMCC-CM to produce the Very High-Resolution Projections for Italy (VHR-PRO_IT) under the RCP8.5 scenario; (2) the Weather Research and Forecasting (WRF) model, driven by

https://doi.org/10.5194/egusphere-2026-4780
Preprint. Discussion started: 19 August 2026

dynamically downscaled EC-Earth global model data under the RCP8.5 scenario, providing a 30-year historical baseline (1979–2008) and future projection (2039–2068); and (3) a WRF hindcast of individual historical observed daily extreme events, forced by ERA5 reanalysis at 0.25° resolution, reconstructing hourly time series of observed extremes over the Misa River basin. A description of all datasets used in this study is provided below

2.2.1 Observational data

The daily observed precipitation records from 1951 to 2023 were obtained from the Istituto Superiore per la Protezione e la Ricerca Ambientale (https://www.isprambiente.gov.it/it). The network comprises six stations that capture the Misa River basin's topographic variability, with higher density in the upstream hilly terrain (Arcevia, Barbara, Colle, and Corinaldo), a mid-basin station (Bettolelle), and a downstream coastal station (Senigallia), illustrated in Fig. 1. Data screening revealed critical gaps: a regional transition from manual to automated instrumentation in 1990 caused a complete data loss across all stations except Arcevia, and Bettolelle lacked multi-decadal data because of its late installation in the 2000s. Therefore, the 1990 data gap and the entire Bettolelle time series were excluded from further processing.

A localized Multiple Linear Regression (MLR) framework was applied to resolve remaining record gaps and construct a continuous daily series suitable for climatological continuity analysis (Portuguez-maurtua et al., 2022; Chang and Burningham, 2024; Al-jahwari et al., 2026). Following spatial dependence protocols (Brunetti et al., 2006), donor gauges for each target station were dynamically selected based on a strict cross-correlation baseline criterion ($r > 0.6$). This setup ensures that missing values are reconstructed using climatologically synchronized neighbors rather than mere geometric distance, which is expected to better preserve upper-tail variance than standard proximity interpolation (Teegavarapu and Chandramouli, 2005). For missing days, an ordinary least squares linear model utilized up to three highly correlated neighboring stations, enforcing a mathematical lower-bound filter to prevent unphysical negative values (Serrano-notivoli et al., 2017).

This transparent, mathematically stable benchmark offers a robust alternative to complex machine-learning approaches, avoiding the associated risk of overfitting, though, as with most gap-filling methods, it moderately smooths the most extreme daily values (Portuguez-maurtua et al., 2022). This approach successfully resolved all minor gaps of Arcevia (0.25%), Corinaldo (0.57%), Colle

https://doi.org/10.5194/egusphere-2026-4780
Preprint. Discussion started: 19 August 2026

(1.93%), Barbara (2.30%), and Senigallia (3.15%) across the catchment network, as shown in Table 1. Cross-validation (Table S1 in the Supplement) indicated residual attenuation of high percentiles (P95/P99, evaluated via percentage bias) and single-day maxima (Rx1day MAE), alongside wet/dry occurrence accuracy assessed via the Critical Success Index. This attenuation was not formally propagated into the Generalized Extreme Value (GEV) for extreme-value analysis and represents an additional source of uncertainty in the resulting return-level estimates.

Finally, a cumulative plot verifies the infilling framework (Fig. S1 in the Supplement), and perfect overlapping across three stations indicates high original data completeness. For the remaining two stations, the upward divergence of the infilled lines in the latter half of the timeline reflects the successful recovery of accumulated rainfall during a data gap, effectively restoring the continuous regional hydrological trend. The 95th percentile threshold graph of these observed data is illustrated in Fig. 2 to show the localized extremes at each meteorological station.

Table 1. Gauge station name, location, period of data covered, active data days, and the proportion of missing data in the Misa River basin. The 1990-year data are excluded in both data period lists and missed data columns.

Station name	Longitude	Latitude	Z (m asl)	Data period	Active data (day)	Total missed data (day)	Missed data (%)
Arcevia	12°56'	43°29'	535	1951-2023	26233	65	0.25
Barbara	13°1'	43°34'	219	1951-2023	25692	606	2.30
Colle	13°3'	43°32	193	1951-2023	25790	508	1.93
Corinaldo	13°2'	43°38'	203	1951-2023	26149	149	0.57
Senigallia	13°12'	43°42'	5	1951-2023	25470	828	3.15

https://doi.org/10.5194/egusphere-2026-4780
Preprint. Discussion started: 19 August 2026

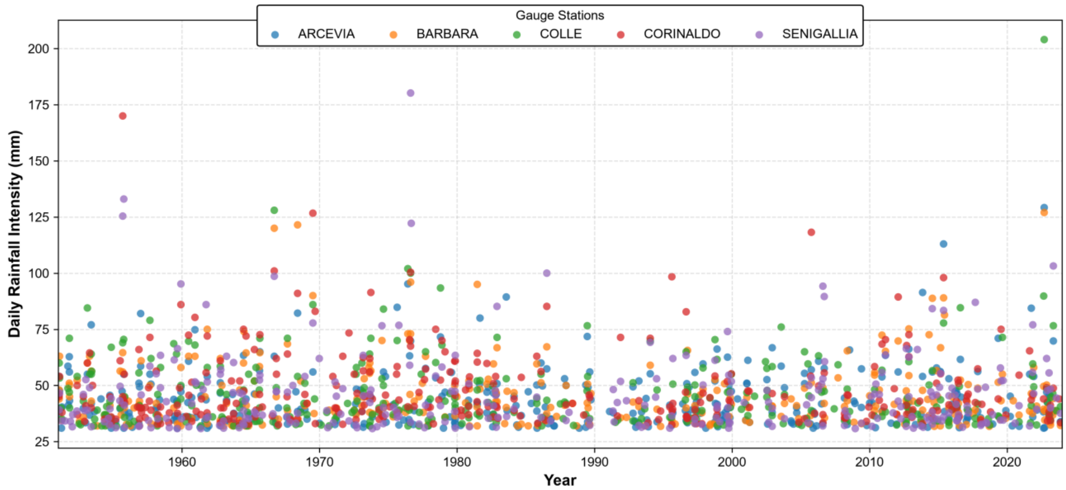

Figure 2. Long-term daily observed rainfall (1951–2023) at the five primary gauge stations (Arcevia, Barbara, Colle, Corinaldo, and Senigallia), identified using an empirical 95th percentile wet-day threshold. The scatter profile establishes the historical upper-tail distribution of localized convective anomalies and synchronized, basin-wide extreme rainfall from gauging stations.

2.2.2 WRF Hindcast of Extreme Events

The catastrophic historical extreme events in the Misa basin between 1940 and the present were hindcasted to reconstruct hourly precipitation distributions because most of them fall outside the model's simulation baseline periods and are in a daily record at the stations. The setup of the model corresponds to the operational WRF at 1.5 km over Italy in the WRF Open Loop (Apicella et al., 2021). The WRF-Open Loop configuration uses three two-way nested domains with horizontal grid spacings of 13.5 km, 4.5 km, and 1.5 km, respectively, and 50 vertical levels. The innermost domain, covering the Italian peninsula at a convection-permitting scale, has 943 × 883 grid points. Initial and hourly lateral boundary conditions are provided by ERA5 reanalysis of 0.25° resolution, providing initial and hourly lateral boundary conditions consistent across the full historical period.

Each historical event was simulated as an individual run initialized 24 hours before the event peak, with a 6-hour spin-up period and and initial and boundary conditions from the ERA5 dataset. The model produces a 48-hour forecast every day, initialized at 00 UTC. The physical parameterization suite includes the Yonsei University scheme for planetary boundary layer turbulence closure, following Hong et al. (2006). Radiation is represented through the RRTMG shortwave and longwave schemes (Iacono et al., 2008). Land-surface processes are represented using the Rapid

https://doi.org/10.5194/egusphere-2026-4780
Preprint. Discussion started: 19 August 2026

Update Cycle land-surface model (Smirnova et al., 1996 and 2000). For cumulus convection, the configuration uses the New Simplified Arakawa–Schubert scheme of Han and Pan (2011) only in the outermost 13.5 km domain. No cumulus parameterization is activated in the 4.5 km and 1.5 km inner domains, because these resolutions are considered able to explicitly resolve convective dynamics. Microphysics parameterization is based on (Thompson et al., 2008).

2.2.3 WRF Climate Simulation

The non-hydrostatic WRF model is used to produce climate change scenarios over the Greater Alpine Region using a convection-permitting domain with 4 km inner resolution (Napoli et al., 2023). Using the EC-Earth global model as initial and boundary conditions and the high-emission scenario (RCP8.5), the study compares a 30-year historical baseline (1979–2008) with future projections (2039-2068) with output at hourly temporal resolution. The setup employs two-way nesting (12 km and 4 km resolutions for the outer and inner domains, respectively) with 50 terrain-following vertical levels and different physical parameterizations, including the Tiedtke convection scheme for the outer domain (Tiedtke, 1989) and the Thompson Aerosol-Aware microphysics (Thompson and Eidhammer, 2014). Furthermore, radiative forcing is managed through the Rapid Radiative Transfer Model for Global (RRTMG) scheme with active greenhouse gas updates (Iacono et al., 2008), while the Yonsei University scheme handles boundary layer transition (Hong et al., 2006).

2.2.4 COSMO-CLM Climate Simulation

The precipitation data used in this study were obtained from the high-resolution climate projection dataset VHR-PRO_IT, generated within the HIGHLANDER project and distributed via the CMCC Data Delivery System (https://dds.cmcc.it, last accessed: 20 July 2026) under a Creative Commons Attribution 4.0 International (CC BY 4.0) license as listed on the DDS platform (DOI: https://doi.org/10.25424/CMCC-J90A-5P12; Raffa et al., 2023), publication date of 01-07-2022. The CMCC DDS temporal-coverage interface lists historical data availability from 1981 and scenario data availability through 2070; data through 2068 were confirmed available and downloaded for this study. This extends beyond the 60 years (1989–2050) described in the original dataset publication (Raffa et al., 2023), on both the historical start and scenario end, indicating that the archived holdings have been extended since publication. For the present study, hourly output was extracted for the historical (1981–2008) and the future RCP8.5 scenario window (2039–2068).

https://doi.org/10.5194/egusphere-2026-4780
Preprint. Discussion started: 19 August 2026

The product was generated at a convection-permitting spatial resolution of ~2.2 km (0.02°) with the regional climate model COSMO-CLM v5.0 (Rockel et al., 2008), dynamically downscaling the global climate model CMCC-CM (via an intermediate 8 km nested step, using INT2LM pre-processing). Physics configurations include single-moment cloud microphysics, two-stream radiation, TKE-based turbulence, the TERRA_ML land-surface model with TERRA-URB urban tiles, and the Tiedtke (1989) scheme with deep convection deactivated.

2.3 Methods

2.3.1 Bias correction for climate modelling data at daily scale

Raw climate model data don't fully align with observed data due to limitations in spatial resolution, parameterization, and local-scale variability (Torma et al., 2015), and bias correction is often recommended to correct the models' systematic errors (Kendon et al., 2012). Despite an improvement in climate model resolution and accuracy, raw outputs still require bias correction against historical observed data to address, among the other modeling errors, the model output tendency to overestimate light rainfall and underestimate intense storms for reliable hydrological use (Menapace et al., 2025; Ivanov et al., 2018). Because hydrological responses such as floods result from extreme rainfall being the main determinant of infrastructure design (Shabestanipour et al., 2024; Mendez et al., 2024), the raw model output can misrepresent the frequency and intensity of extreme rainfall (Sun et al., 2006; Teutschbein and Seibert, 2012). Therefore, an initial and essential step involves adjusting model outputs using reliable ground-based observational datasets to obtain more accurate extreme rainfall results.

In this study, a point-to-grid bias-correction framework was applied to correct the daily total precipitation projections from the high-resolution regional climate model simulation (Bannister et al., 2019; Derdour et al., 2022). The hourly model data were at first temporally aggregated to daily totals to ensure a consistent training baseline with the observations. Spatially, point-based rain gauge observations were first aligned with raw model outputs via nearest-neighbor interpolation to extract the localized climate time series corresponding directly to each station location. At these point coordinates, Quantile Delta Mapping (QDM) was executed to preserve local storm variance against the smoothing effects of spatial interpolation (Maraun, 2013). QDM is a trend-preserving method that adjusts systematic biases in model series relative to observations while explicitly maintaining the model-projected relative changes (deltas) in all quantiles (Cannon et al., 2015), an

https://doi.org/10.5194/egusphere-2026-4780
Preprint. Discussion started: 19 August 2026

approach that has been shown to achieve significant reductions in systematic bias (Bangelesa et al., 2026).

Prior to calibration, a wet-day precipitation of a 0.1 mm d^{-1} step threshold was applied to eliminate drizzle noise. Following the multiplicative QDM configuration, empirical cumulative distribution functions (CDFs) were evaluated across 50 monthly quantiles; the simulated values were bias-corrected using quantile mapping transfer functions constructed during the baseline periods, and the projected relative rainfall change (ratio) in quantiles is multiplied by the bias-corrected baseline values using Eq. (1). To reconstruct a continuous gridded dataset across the entire model domain, Inverse Distance Weighting (IDW) was subsequently employed to spatially correct the data generated for each station. A distance-decay parameter (p = 2) was applied to represent the diminishing spatial influence of each station with increasing distance (Lu and Wong, 2008), reducing local distributional bias.

$$\hat{x}_{m,f}\,(t) = F^{-1}_{o,h}\left\{F_{m,f}\left[x_{m,f}(t)\right]\right\} * \frac{x_{m,f}(t)}{F^{-1}_{m,h}\left\{F_{m,f}\left[x_{m,f}(t)\right]\right\}} \qquad (1)$$

where:
$\hat{x}_{m,f}\,(t)$ is the final bias-corrected future model prediction at time step t; $x_{m,f}\,(t)$ is the raw future model simulation value at time step t; $F_{m,f}$ is the cumulative distribution function (CDF) of the simulated variable from the future model period; $F_{m,f}\left[x_{m,f}(t)\right]$ is the non-parametric percentile corresponding to the raw future value within its own future distribution; $F^{-1}_{o,h}$ is the inverse CDF of the historical observations; $F^{-1}_{m,h}$ is the inverse CDF of historical model simulation; $F^{-1}_{o,h}\left\{F_{m,f}\left[x_{m,f}(t)\right]\right\}$ is the historical observed value that corresponds to the same percentiles as the future model value; and $F^{-1}_{m,h}\left\{F_{m,f}\left[x_{m,f}(t)\right]\right\}$ is the historical model value that corresponds to the same percentiles as the future value.

As presented in Haerter et al. (2011), the corrected daily values were disaggregated to an hourly resolution by applying the relative diurnal fractions of the original model output. To restore the hourly resolution required for impact analysis, a mass-conservative method of fragments was applied. In this step, hourly fractions were calculated from the original raw model and used to distribute the corrected daily totals, ensuring that the final hourly rainfalls reflect the corrected daily volume while respecting the model's internal physical timing (Haerter et al., 2011; Nguyen et al., 2024). This approach helps to remove systematic errors in the model by maintaining the physical consistency of sub-daily precipitation patterns at a more statistically robust daily scale, as reported by Haerter et al. (2011). This methodology ensures the best mass-balance consistency and provides a robust foundation for analyzing hourly rainfall, as the magnitude shift from the QDM

https://doi.org/10.5194/egusphere-2026-4780
Preprint. Discussion started: 19 August 2026

process is fully integrated into the sub-daily temporal structure (Westra et al., 2012). Finally, the model output of the temporal distribution of before- and after-bias correction was verified for some extreme hours, and the result shows it fully follows the original sequence of time distribution (Fig. S3). This hourly temporal distribution is fundamentally important to study future extreme events.

2.3.2 Climatology and extreme rainfall event analysis

In this study, the mean annual and seasonal precipitation were calculated over the reference period (1979–2008 for WRF and 1981–2008 for COSMO) and the future period (2039–2068). Then, the future changes were computed at each grid point as a relative percentage difference with respect to the reference period. The use of two different reference periods is dictated by the data availability on the CMCC DDS online server. For the climatological analyses presented in this study, the absence of the first two years of the historical simulation for COSMO is not expected to have a significant impact on the results. This multi-period comparison provides the primary analytical framework for detecting nonstationary shifts in the seasonality, timing, and intensity of daily precipitation, enabling direct comparison between historical and future projected climate conditions (Sharif et al., 2025).

Moreover, the daily maximum precipitation for each year in the domain was extracted and calculated for both the historical and future periods of the model. The resulting annual maxima were fitted with the GEV distribution through the method of maximum likelihood estimation. The GEV distribution is well known for extreme analysis due to its flexible three-parameter formulation that can capture bounded, heavy-tailed, and light-tailed extreme behaviors without threshold-selection biases (Coles, 2001; Papalexiou and Koutsoyiannis, 2013). This statistic is consistent with standardized methods employed to assess the representation of extreme threshold failures of climate models and the shifts of infrastructural risk across various historical and future horizons (Amir et al., 2013; Kao and Ganguly, 2011). To verify the fitted theoretical frequency curves, an empirical return period for unbiased simulated and observed data was calculated using the Gringorten plotting position (Gringorten, 1963).

95% confidence intervals for benchmark return periods were estimated via non-parametric bootstrap (2000 iterations) on the annual maximum series for both observed and modeled datasets, re-estimating GEV parameters by maximum likelihood for each replicate. For a fixed benchmark magnitude, the return period was recalculated for each replicate by evaluating its exceedance

https://doi.org/10.5194/egusphere-2026-4780
Preprint. Discussion started: 19 August 2026

probability under the re-estimated parameters, with the 2.5th–97.5th percentiles across replicates defining the confidence interval. Following Overeem et al. (2008), this data-driven approach quantifies sampling uncertainty without assuming parameter normality. For benchmark events, the observed return period was estimated from the historical record, and the corresponding future return period was derived by evaluating exceedance probability under the projected model distribution.

The intensity changes of return period events were quantified as relative percentage changes between historical model outputs and future projections under RCP8.5 for both models to assess how climate change alters extreme daily rainfall magnitude. Subsequently, changes in daily event frequency were evaluated using a non-stationary probability mapping approach (Eq. 2). For each historical return period event (T_{hist}), the corresponding rainfall quantile was extracted from the fitted historical GEV distribution. This quantile was then mapped onto the future GEV distribution to determine the future return period (T_{fut}); that is, how frequently the same rainfall magnitude would occur under future climate conditions. This approach follows the probability mapping formulation of Kao and Ganguly (2011) and Salas et al. (2014), which directly compares historical and future extreme value distributions without requiring arbitrary threshold selections, thereby capturing the full non-linear amplification of exceedance frequencies across the return period spectrum.

$$T_{fut} = \left[1 - \exp\left(-\left(1 - \xi_{fut}\left(\frac{F_{hist}^{-1}\left(1-\frac{1}{T_{hist}}\right)-\mu_{fut}}{\sigma_{fut}}\right)\right)_{+}^{\frac{-1}{\xi_{fut}}}\right)\right]^{-1} \qquad (2)$$

where: T_{fut} is the risk-accelerated future return period (years); T_{hist} is the baseline historical design return period (years); F_{hist}^{-1} is the inverse CDF fitted to the historical baseline series; μ_{fut}, σ_{fut}, ξ_{fut} are the location, scale, and shape parameters, respectively, of the fitted future projection GEV distribution.

To define events relevant to impact analysis, two complementary sources were considered: climate model outputs projecting potential future changes over the study area and eight historically observed extreme events recorded in the basin. The historical events were identified from flood records spanning different periods, as documented in Giuseppe and Rossano (2021), and represent major flood episodes previously observed in the region. These historical events were subsequently simulated using the WRF model to reconstruct their hourly precipitation distribution (see Fig. S4

https://doi.org/10.5194/egusphere-2026-4780
Preprint. Discussion started: 19 August 2026

in the Supplement). To characterize each event and identify analogous occurrences in future climate projections, the threshold-based event screening framework by fixed-rank selection was employed, an extreme value method that statistically analyzes exceedances above a defined threshold (Brunner et al., 2020; Volpi et al., 2015). For this study, a minimum daily precipitation threshold of 70 mm in the basin peak was adopted, corresponding to the lower bound of daily extremes associated with historical flooding in the basin. Using this threshold of basin peak value, future extreme rainfall events were extracted directly from the climate model outputs and compared with historical extreme events in the basin.

These extracted upper-tail extremes from the top-selected events are used directly to analyze the temporal structure of sub-daily rainfall. As presented in Shepherd et al. (2018) and Feser and Shepherd (2025), it shows that a direct-use, model-derived approach to extreme sub-daily output can preserve physically consistent storylines, improving risk awareness; providing a physical basis for partitioning uncertainty; and strengthening decision-making while avoiding the structural uncertainties and artificial temporal patterns associated with traditional extreme-value distribution fitting. The top selected events of the tail values of future extremes and historical hindcasted extremes were then further analyzed to identify the hourly spatial-temporal distribution of real storms, rather than assuming statistical symmetry.

For each extreme event, a nine-hour storm window centered on the peak hourly intensity was extracted to identify the maximum hourly intensity and the cumulative extreme rainfall accumulation, which are essential for characterizing the time to peak across the basin. Because most historical sub-daily extreme rainfall events that cause flood hazards in the Misa River basin last less than nine hours, this window mostly captures the largest peak of runoff-generating rainfall. It also isolates the active core storm, where nearly all extreme rainfall mass and peak intensity occur, while excluding the low-intensity tails of the broader 24-hour period. The cumulative rainfall values were then fitted to a two-parameter logistic (sigmoidal) function via non-linear least squares regression (Virtanen et al., 2020), following the general approach of parametrizing normalized extreme mass curves established by Koutsoyiannis and Foufoula-Georgiou (1993).

This approach enabled a standardized comparison of storm accumulation dynamics across historical hindcast and future scenarios through two key parameters: the location parameter (μ), representing the timing of maximum accumulation rate, and the scale parameter (s), describing the steepness of the accumulation curve. Additionally, the normalized Huff Curve method (Huff, 1967) was applied to characterize the cumulative temporal distribution of rainfall within each extreme event, expressed as dimensionless percentages of both total extreme event duration and its depth. This approach distributes storm mass into quartiles, enabling identification of shifts in intra-storm rainfall timing across climate scenarios (Bonta, 2004; Zambrano et al., 2026). A Huff curve shifting toward the first quartile indicates a transition toward front-loaded, more sudden rainfall release, while a shift toward later quartiles reflects increasingly back-loaded storm structures that are more prone to rainfall hazards in catchments (Zambrano et al., 2026), providing a standardized fingerprint of extreme event behavior across different climate regimes.

3. RESULTS AND DISCUSSION

3.1 Daily Precipitation

3.1.1 Model validation and climate characterization of the catchment

The empirical CDFs and heavy-tailed daily rain (P99) reveal strongly contrasting structural biases between the two models across the Misa River basin in the historical reference period. The basin average summary statistics in Table S2 in the Supplement for Fig. 3 show that the raw COSMO simulation consistently underestimates rainfall throughout the precipitation spectrum, with the P99 reaching only 32.15 mm d^{-1} of basin average compared to the observed 40.24 mm d^{-1}. This underestimation across the precipitation spectrum reflects the well-known dry bias of convection-permitting models and the tendency of regional models to underpredict precipitation intensities over Italy's complex terrain (Bucchignani et al., 2016). In contrast, raw WRF substantially overestimates heavy precipitation events, with a P99 of 46.92 mm d^{-1} and a basin average maximum of 98.67 mm d^{-1} against the observed maximum of 70.64 mm d^{-1} of the same model period data.

The comparison of extreme rainfall percentiles (90th, 95th, and 99th) values between observed data and model simulations of raw and bias-corrected using a <4 km buffer surrounding each gauging station were examined (see Table S3 in the Supplement). Overall results show that raw model outputs show clear biases, with WRF overestimating and COSMO underestimating the observed extreme rainfall percentiles. The application of bias correction substantially reduces these disparities across all stations, aligning model estimates closely with observational data. As presented in Prein et al. (2015), a WRF's overestimation is consistent with the known 'gray-zone' limitation of convection-permitting configurations, where finer grid spacings (<4 km) remain insufficient to fully resolve individual convective updrafts, producing excessive grid-scale convective amplification over steep orographic terrain.

Because both WRF and COSMO resolve convection explicitly rather than relying on parameterization, they are well suited to representing precipitation extremes more realistically than coarser parameterized models, yet their opposing biases show that convection-permitting resolution alone does not eliminate structural model uncertainty in extremes (Pichelli et al., 2021). Therefore, quantile-based bias correction realigns both models with the observed baseline, reducing the underestimation in COSMO and overamplification in WRF (Fig. 3a, 3c), while residual biases remain.

In addition, mean annual (Fig. 4) and seasonal precipitation (see Fig. S2 in the Supplement) in the Misa catchment are characterized by higher cumulative daily precipitation in mountain areas compared to coastal areas in all the seasons, while both WRF and COSMO exhibit significant geographic and absolute amplitude biases prior to correction mainly in summer and autumn (see Fig. S2 in the Supplement). The changes were observed in the annual delta map of the WRF model in the grids, ranging from -0.55 mm d^{-1} to +0.035 mm d^{-1}, whereas all positive deltas were over 0.3 mm d^{-1} for the COSMO model delta (Fig. 5). In seasonal cases, summer and autumn show positive corrections exceeding +0.1 mm d^{-1} for WRF and over +0.4 mm d^{-1} for COSMO, whereas they have a negative delta (over -0.8 mm d^{-1}) in spring for both model grids (Fig. S2 in the Supplement).

As presented by Cardoso et al. (2012), WRF generally overestimates annual and seasonal rainfall except autumn, where it underestimates and struggles with convective rainfall over small coastal watersheds. The similar behavior observed in this study of both models results in underestimating all three seasons except spring, where it overestimates. Thus, quantile-based correction tried to resolve localized seasonal amplitude discrepancies across the model grid while preserving the physically coherent spatial gradients generated by each model's atmospheric core. By accurately reproducing the observed baseline in both COSMO and WRF historical simulations, this approach demonstrates its ability to reduce systematic errors without disrupting temporal dynamics.

https://doi.org/10.5194/egusphere-2026-4780
Preprint. Discussion started: 19 August 2026

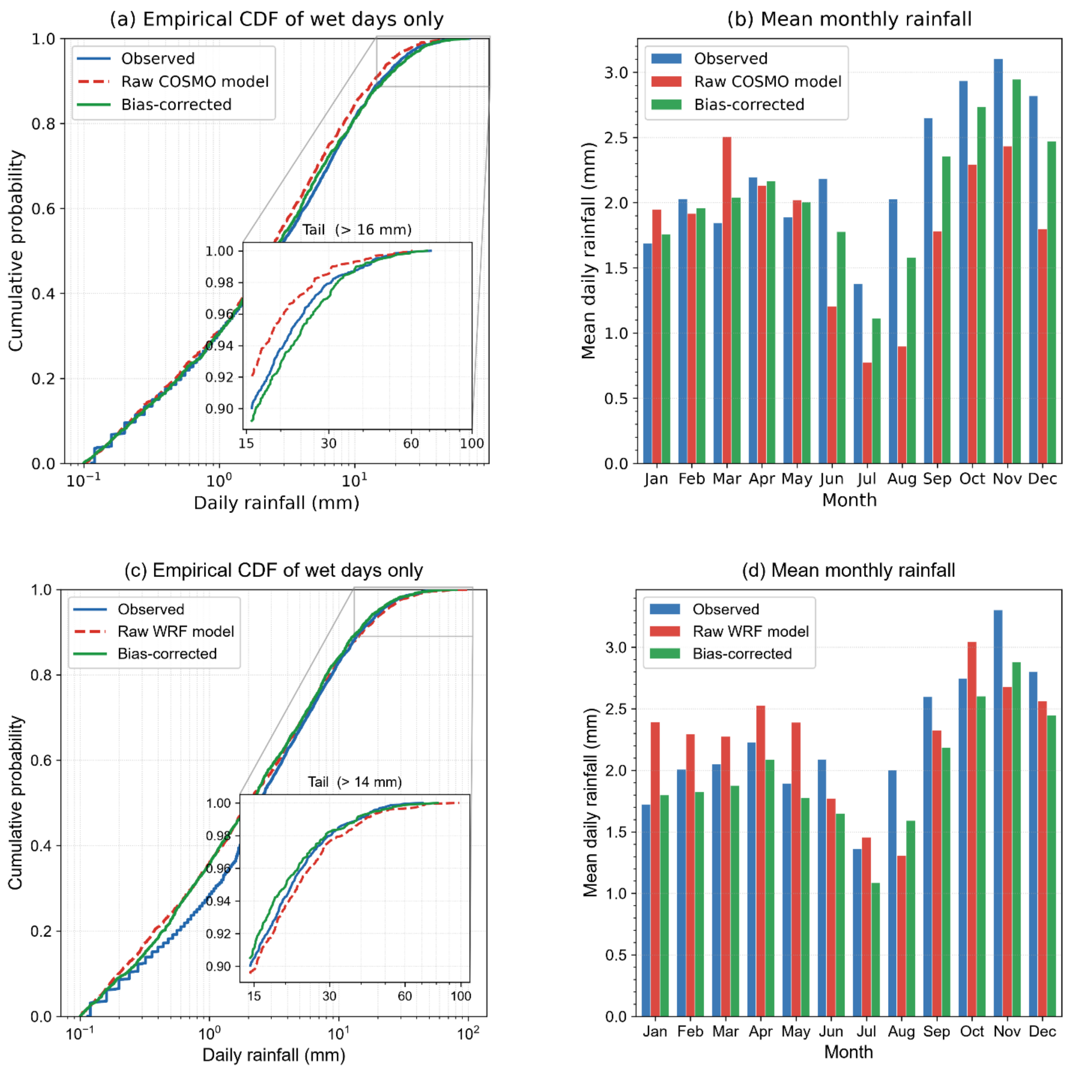

Figure 3. Historical models of COSMO and WRF validation with observed data: The raw model (red line/bar), observed (blue line/bar), and corrected model (green line/bar) on the empirical CDF of wet-days (>0.1 mm d^{-1}) rainfall graph (**(a)** and **(c)**) and the all-day mean monthly rainfall graph (**(b)** and **(d)**) for the 1979/81–2008 historical period.

https://doi.org/10.5194/egusphere-2026-4780
Preprint. Discussion started: 19 August 2026

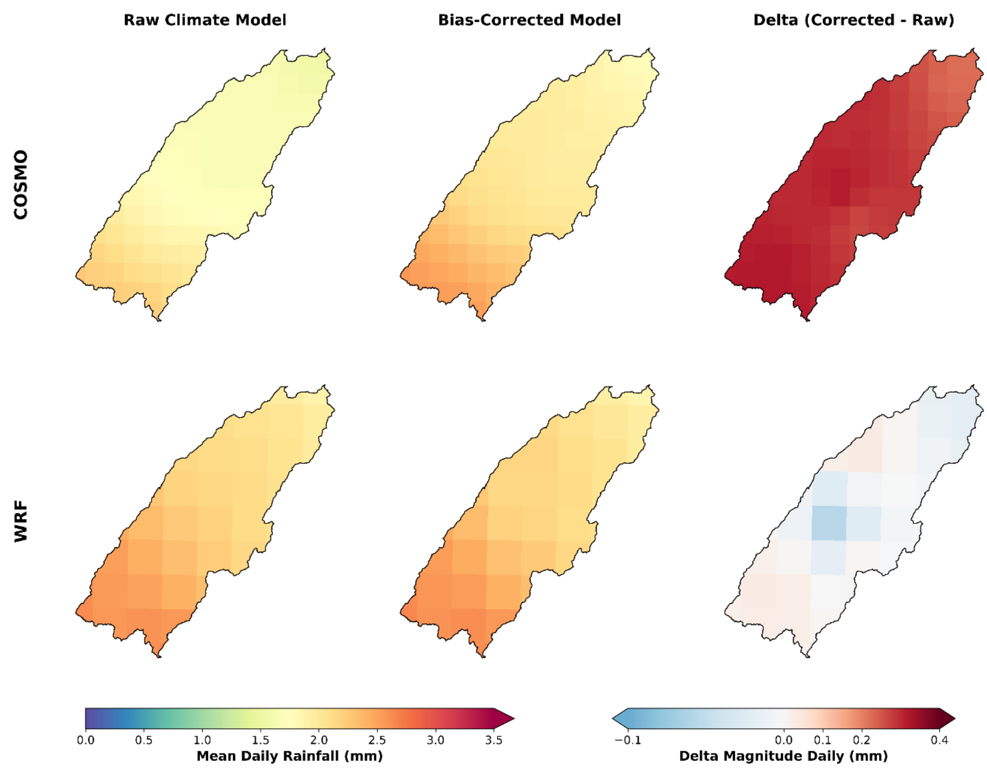

Figure 4. Mean daily precipitation (mm d^{-1}) during the historical period (1979/81–2008) for the raw and corrected climate simulations, COSMO (first row) and WRF (second row), as well as the change between the corrected and raw maps over the Misa River basin.

3.1.2 Future climate over the basin

The annual climate change signal represented in Fig. 5 shows an overall decrease in mean annual precipitation over the Misa catchment under the RCP8.5 scenario for both models, though they differ substantially in spatial magnitude: while COSMO projects an annual reduction ranging from 0% to −5%, WRF projects a more pronounced drying signal from −5% to −20%. Both simulations show larger absolute changes in mountainous areas than in coastal lowlands. Seasonal spatial maps reveal marked intra-annual divergence between the two models (Fig. 6). Both models converge on a persistent summer drying signal; however, this signal is substantially more pronounced in WRF, where summer precipitation reductions exceed −30%, while COSMO exceeds −20%. As shown in Fig. 6, the two models diverge during the other seasons; COSMO projects wetter winter and autumn conditions (approximately 0% to +15%) alongside moderate spring drying (approximately

https://doi.org/10.5194/egusphere-2026-4780
Preprint. Discussion started: 19 August 2026

−5% to −15%), whereas WRF projects precipitation decreases during winter and autumn (approximately −5% to −15%) but a spring increase (approximately 0% to +10%). Despite these inter-model differences, both models indicate an overall decrease in future annual precipitation over the catchment (see Fig. 5).

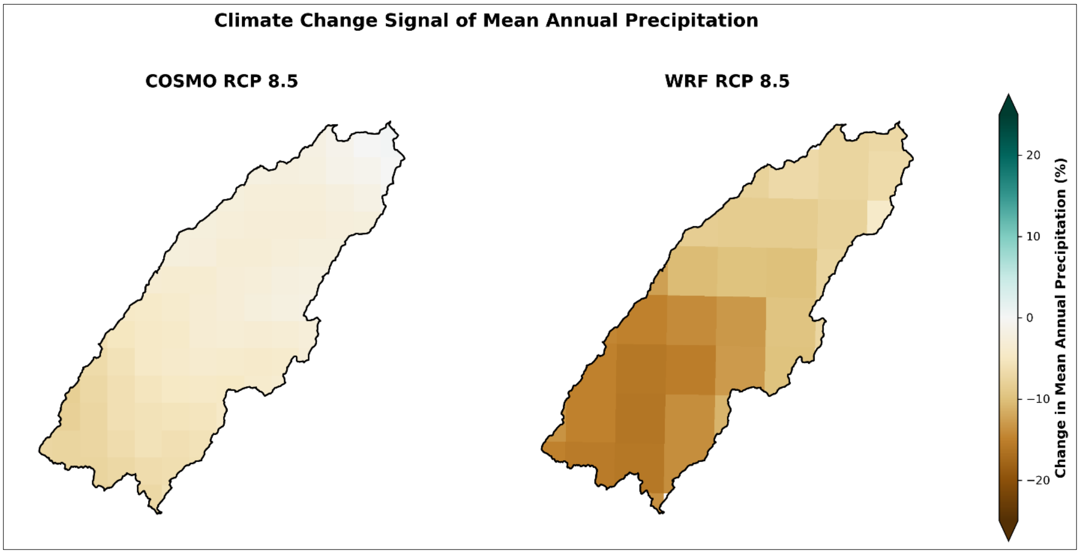

Figure. 5. Relative mean annual precipitation changes in percentage between future (2039–2068) under the RCP8.5 scenario and historical (1979/81–2008) periods for the COSMO and WRF models.

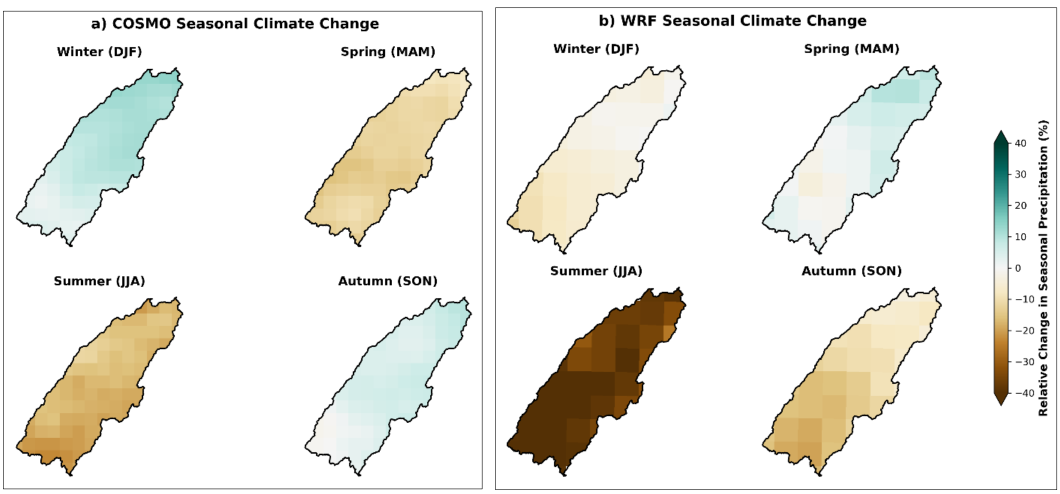

https://doi.org/10.5194/egusphere-2026-4780
Preprint. Discussion started: 19 August 2026

Figure 6. Relative changes in percentage of the mean seasonal precipitation between the future (2039-2068) under the RCP8.5 scenario and the historical (1979/81-2008) periods for COSMO **(a)** and WRF **(b)** models

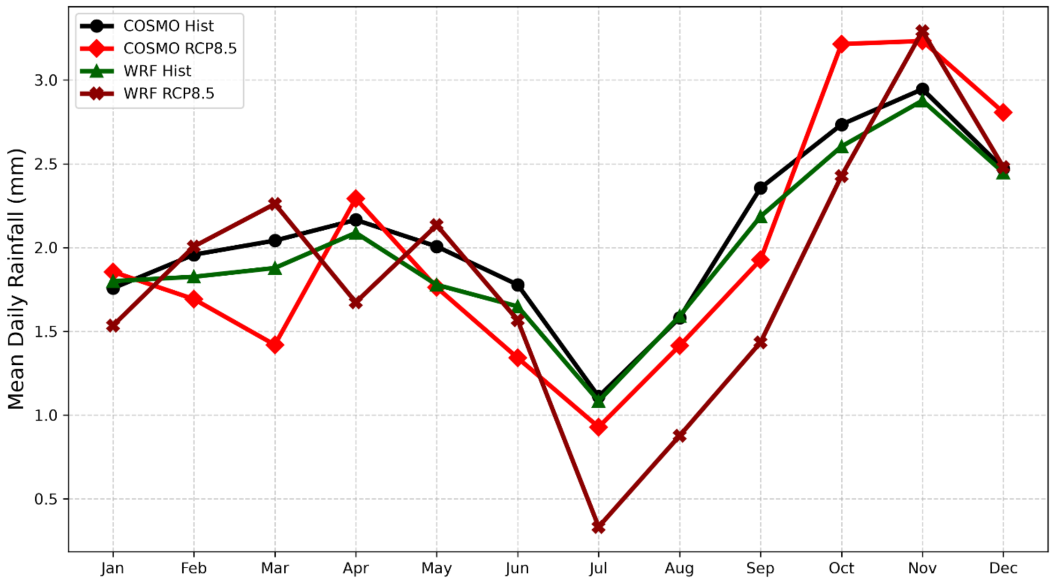

Figure 7. Monthly mean daily precipitation (mm d^{-1}) averaged over the catchment, comparison under the historical model periods (1979/81-2008) and future projection period (2039-2068): COSMO model results of the black line (historical) and light red line (RCP8.5); and the WRF model results of the green line (historical) and brown line (RCP8.5)

As shown in Fig. 7, the basin-averaged seasonal climatology reveals a distinct bimodal regime, characterized by an absolute dry minimum in July, a primary peak in autumn, and a secondary peak in spring (April). Under RCP8.5, both models project drier summers, with July rainfall decreasing further, alongside an intensification of the autumn peak. A notable inter-model divergence emerges during spring, where WRF projects substantially wetter March conditions while COSMO indicates a drying trend. Moreover, the point-to-grid analysis of basin climatology reveals that almost all gauging stations are converging with historical model data (see Fig. S5 in the Supplement). However, some gap between observations and modeled historical data is found for the WRF model, specifically at the Arcevia, Corinaldo, and Senigallia stations. At these stations, the WRF historical model underestimates, whereas the COSMO historical model is closer to the observations. Overall, both models underestimate summer precipitation, while under future

https://doi.org/10.5194/egusphere-2026-4780
Preprint. Discussion started: 19 August 2026

conditions, they show a climatological divergence in March and April at all gauging stations and on the basin-wide average. The main climatological finding is that both models project the mean daily precipitation to increase in November and be reduced in summer under future climate conditions (Fig. 7).

3.1.3 Daily extremes and benchmark events

i) Simulated extremes

The multi-model projections detailed in Table 2 and represented in Fig. 8 indicate a consistent increase in daily precipitation intensities across return periods under RCP8.5. Table 2 shows that the COSMO projects a progressive amplification of precipitation intensity ranging from +34.81% for the 10-year return period to +67.11% for the 500-year threshold. In addition, WRF projects a more uniform increase across return periods, with amplification ranging from +50.36% at the 10-year level stabilizing to +43.06% at the 500-year threshold. Thus, the projected magnitudes and incremental directions of two models differ, but overall, both models consistently project an increase in the intensity of daily precipitation extremes over the catchment. When expressed in terms of exceedance frequencies, these increases in magnitude imply that events previously associated with long return periods become more frequent. As shown in Table 2, a historical daily precipitation event with a 100-year return period is projected to have a return period of just 4.8 years under COSMO and 9.4 years under WRF. This suggests it could become 10 to 20 times more frequent under future climate conditions, representing a dramatic increase in the frequency of such daily events.

Both models indicate daily precipitation intensity increases in the range of 47.11–54.31% for the 100-year event (Table 2). These projections are consistent with previous findings showing that under RCP8.5, the daily extreme precipitation events will intensify and substantially become more frequent under warming climates (Dahm et al., 2019; Faggian, 2021). As shown in this study, both models exhibit an amplified increase in frequency for rarer events under future climate. This highlights a non-uniform shift in the precipitation probability distribution, where extreme tail events intensify at a higher rate than moderate occurrences, leading to disproportionate amplification of high period events compared to the bulk of precipitations (Myhre et al., 2019). Events occurring once per generation may therefore occur multiple times within a single

https://doi.org/10.5194/egusphere-2026-4780
Preprint. Discussion started: 19 August 2026

operational decade, with significant implications for designed thresholds under traditional stationary frameworks (Salas et al., 2014).

Table 2. For each return period (Tr) in years of daily extreme (mm d^{-1}), the table shows the model relative intensity changes and exceedance frequency shifts (risk acceleration) of historical (1979/81–2008) and future (2039–2068) simulations under RCP8.5.

RCP8.5 Intensity Changes (Δ%)							**Exceedance Frequency Shift**	
Tr (yr)	COSMO Hist (mm d^{-1})	COSMO Fut (mm d^{-1})	COSMO Δ (%)	WRF Hist (mm d^{-1})	WRF Fut (mm d^{-1})	WRF Δ (%)	COSMO Fut Tr (yr)	WRF Fut Tr (yr)
10	85.44	115.19	+34.81	85.49	128.53	+50.36	2.5	2.0
50	96.66	143.67	+48.63	113.78	168.96	+48.51	4.0	5.6
100	100.36	154.87	+54.31	126.89	186.68	+47.11	4.8	9.4
200	103.56	165.57	+59.88	140.70	204.71	+45.49	5.6	16.2
500	107.12	179.01	+67.11	160.13	229.09	+43.06	6.6	35.2

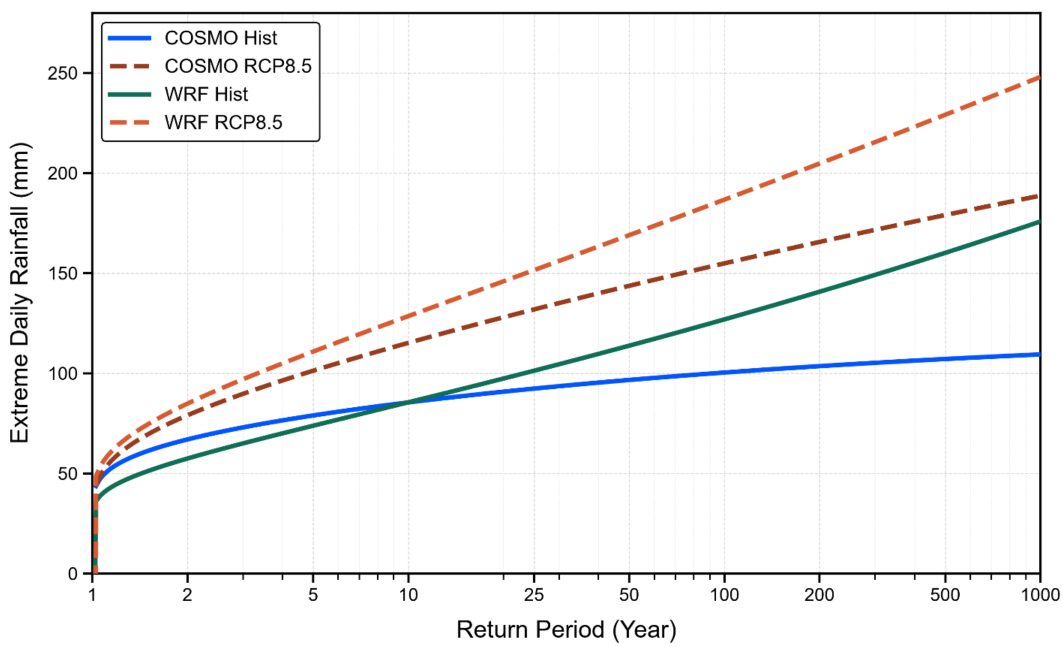

Figure 8. Daily extreme precipitation of basin-max and its return periods for the model simulations (1979/81–2008, 2039–2068): the extreme rainfall return periods' fit lines graph of the COSMO historical model (blue line), WRF historical model (green line), COSMO RCP8.5 (dark broken red line), and WRF RCP8.5 (light broken red line).

https://doi.org/10.5194/egusphere-2026-4780
Preprint. Discussion started: 19 August 2026

ii) Basin-wide maxima of models and observations relative to historical benchmark events

To assess whether historically observed daily extreme precipitation events that caused flooding in the catchment could recur under future conditions, the return periods of basin-maximum daily precipitation were evaluated, with sampling uncertainty quantified via 95% bootstrap confidence intervals. From the eight selected extreme events, the five most flood-productive events, such as Sept 1955, Aug 1976, Dec 1982, May 2014 and Sept 2022, were examined against future extreme return periods from both models (Fig. 9 and Table 3). Comparing documented flood-producing benchmarks with future distributions reveals divergent model responses rather than a uniform hazard increase: WRF projects an increased likelihood across all benchmark magnitudes, whereas COSMO projects higher frequencies for moderate events but reduced frequencies for the highest-magnitude extremes in the Misa River basin (Fig. 9). The catastrophic September 2022 event (basin-maximum of 204.0 mm d^{-1} recorded by rain gauges), which has an estimated return period of 182 years under the observed historical GEV baseline, shows markedly divergent future projections between the two models (Table 3). Under the WRF for future projection, its recurrence interval is nearly halves to roughly 97 years, effectively doubling its annual probability of occurrence.

Conversely, the COSMO projection shifts this extreme to an 860-year return period threshold, suggesting that this event is represented as substantially rarer in COSMO; nevertheless, the observed event magnitude remains well within the wide 95% bootstrap confidence interval of both future climate projections. While WRF projects a sharp acceleration in risk for the high-magnitude September 1955 (170.0 mm d^{-1}) and August 1976 (180.2 mm d^{-1}) benchmarks, COSMO projects that events of these magnitudes become less frequent in the future period. The historical 1976 storm, originally a severe, nearly 94-year hazard, is projected by WRF's central estimate to reduce to approximately a 46-year event, a shift that, if realized, would mean such magnitudes recur multiple times within a standard infrastructure design life, though this point estimate carries substantial uncertainty. Similarly, the 1955 storm has an estimated return period of 69 years, which decreases to a 34-year threshold in WRF and remains a highly stable, nearly 79-year event in COSMO.

However, these point estimates are accompanied by very wide upper-tail uncertainty: confidence intervals for large-magnitude events extend from a few decades to more than 1000 years. The 182-

, 97-, and 860-year estimates discussed above should therefore be interpreted cautiously as central tendencies rather than precise predictions. The central finding is not the exact recurrence of intervals themselves, but that central estimates diverge systematically between models, while the available historical record remains too short to tightly constrain the upper tail of the distribution. This threshold-dependent shift indicates that while future climate envelopes reflect increased probabilities of moderate flood-producing events, the frequency of severe high-tier extremes depends strongly on model dynamics: WRF projects a widespread shift toward higher event frequencies, whereas COSMO projects reduced occurrence rates for the most severe historical thresholds.

The changes in extreme event frequency are heavily supported by recent localized extreme value analyses conducted across flood-prone basins in Italy. Maines et al. (2026) evaluated the historic October 2018 Vaia storm in northeastern Italy and demonstrated that the return period of its precipitation event is projected to be nearly halved at future global warming levels, supporting the reduction in return periods identified in our projections. Furthermore, Gentilucci et al. (2023) utilized GEV profiling on the Adriatic slope of Central Italy to show that recent convective anomalies, specifically including the September 2022 storm, indicate departures from historical stationarity assumptions. While the future shift in COSMO for the September 2022 event presents a contrast in tail-extension behavior, the broader literature supports the relevance of assessing how historical extreme magnitudes are repositioned within future extreme-value distributions.

Shifting from a basin-wide maximum to station-level extraction reveals spatial variability that an aggregated proxy obscures (Fig. S6 in the Supplement). At Corinaldo, the historical 100-year threshold falls to 146.9 mm d^{-1} (COSMO) versus 106.6 mm d^{-1} (WRF), while projected 500-year rainfall reaches 209.6 mm d^{-1} (COSMO) versus only 117.6 mm d^{-1} (WRF), reflecting model sensitivity in representing convective processes (Ban et al., 2014, Prein et al., 2015). Station-level return periods are also highly sensitive to whether a storm core directly struck a given gauge: the September 2022 event yields a return period exceeding 1000 years at Colle (204.0 mm d^{-1}) but only 135 years at Arcevia (129.2 mm d^{-1}), decreasing to 47–75 years under future projections (see Fig. S6 in the Supplement). Similarly, the 1976 storm exceeds 1000 years historically at Senigallia but drops to 112–173 years under future conditions, while the 1955 storm at Corinaldo diverges sharply between models (193 years under COSMO vs. >1000 years under WRF). This instability

https://doi.org/10.5194/egusphere-2026-4780
Preprint. Discussion started: 19 August 2026

reflects the mixed-population problem in extreme value, where a single distribution is fitted to records shaped by both stratiform and localized convective extremes (Dallan et al., 2022 and 2024; Blöschl et al., 2019), consistent with findings by Gentilucci et al. (2023), on the Adriatic slope. Basin-wide maxima therefore characterize catchment-scale upper bounds for general planning, while station-level analyses remain essential for diagnosing site-specific design vulnerabilities (Kao and Ganguly, 2011; Salas et al., 2014).

Table 3. The daily observed extremes of five events from the eight and their return periods (Tr) comparison under historical observed period of 1951-2023 (N = 72) and future period of 2039-2068 (N = 30) scenarios under RCP8.5. 95% bootstrap confidence interval results for return periods are presented as Value [Lower-Upper]; return period estimates exceeding 1,000 years are capped at >1000 years for numerical stability and interpretability.

Event	Obs. (mm d^{-1})	Tr Obs. (yr)	Tr COSMO Fut (yr)	Tr WRF Fut (yr)
Sep-1955	170.0	69.0 [12.9 – >1000]	79.3 [36.2 – >1000]	33.5 [19.9 – >1000]
Aug-1976	180.2	93.6 [16.1 – >1000]	152.8 [49.5 – >1000]	46.4 [23.5 – >1000]
Dec-1982	85.2	3.1 [1.9 – 4.4]	1.7 [1.5 – 4.1]	1.9 [1.4 – 3.2]
May-2014	90.4	3.9 [2.1 – 5.6]	1.9 [1.8 – 5 .4]	2.3 [1.5 – 4.0]
Sep-2022	204.0	181.9 [24 – >1000]	860.1 [86.3 – >1000]	96.8 [39.0 – >1000]

https://doi.org/10.5194/egusphere-2026-4780
Preprint. Discussion started: 19 August 2026

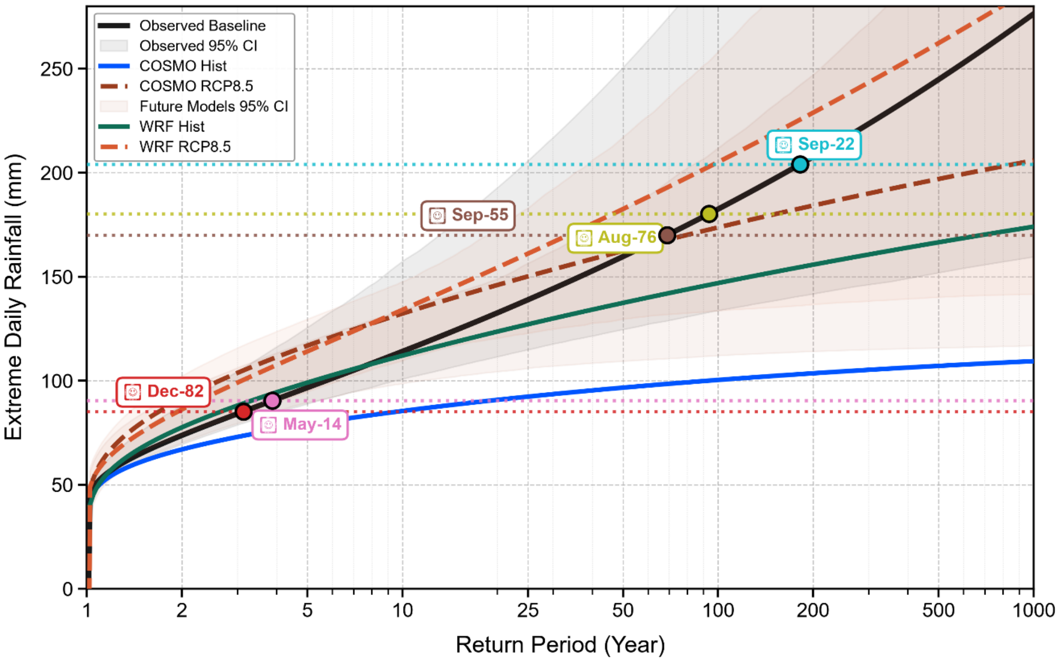

Figure 9. Daily extreme rainfall of basin-max and its return periods for the historical observed (1951–2023), historical models (1979/81–2008), and future (2039–2068) data. The extreme rainfall returns periods' fit lines graph of the COSMO historical model (blue line), WRF historical model (green line), COSMO RCP8.5 (dark broken red line), WRF RCP8.5 (light broken red line), and historical benchmark extreme events (horizontal broken lines)

3.2 Hourly precipitation: Top Eight Extreme Rainfall Events

3.2.1 The spatial-temporal analysis of extreme events

To evaluate changing event-scale dynamics across the Misa River basin, a peak-centered normalized nine-hour temporal concentration of the peak hourly intensities was extracted for the top eight extreme rainfall events from both the historical hindcast and the future extreme scenarios of the 2039–2068 period (Fig. 10). The rationale behind the 9-hour duration is discussed in detail in Sect. 3.2.3. This analysis characterizes how peak intensification and event-scale variability evolve under future climate conditions compared to the past, offering a short-duration, spatial-temporal perspective essential for understanding how extreme rainfall patterns drive hazards in the catchment. Future projections reveal contrasting changes between the two models rather than a consistent increase in event magnitude relative to the historical baseline. Under the COSMO RCP8.5 scenario, maximum hourly intensities reach 79.37 mm h^{-1} (E08), an increase of +11.6%

https://doi.org/10.5194/egusphere-2026-4780
Preprint. Discussion started: 19 August 2026

compared to the historical maximum event (Table 4 and Fig. 10). Conversely, WRF future projections show a reduction of up to -9.4% (E02) in maximum peak intensity compared to historical events (Table 4).

This reduction may reflect model uncertainty in capturing localized convective hotspots at the sub-basin scale and a limitation of convection-permitting simulations in complex coastal-mountain terrain, discussed further below (Prein et al., 2015). In addition, in COSMO, the event with the maximum peak intensity (E08) also corresponds to the event with the maximum cumulative precipitation depth, whereas in both WRF and the historical dataset, the events with maximum peak intensity and maximum cumulative depth do not coincide. These contrasting responses between COSMO and WRF highlight the uncertainty associated with the representation of future precipitation extremes at the basin scale, particularly for localized, high-impact events in complex mountainous regions. Further investigation of the underlying physical mechanisms is needed to attribute these differences to changes in convective processes or storm structure.

The temporal concentration of the normalized 9-hour accumulation extremes and their hyetographs show that historical sub-daily extremes tend to be front-loaded, with rainfall concentrated in the first 1–5 hours (Fig. 10a). Note that front-, center-, and back-loaded storms are classified by peak timing within the first, middle, or final third of the 9-hour window (measured from its start), respectively. The September 2022 event is the clearest example: it was entirely front- and center-loaded, with no rainfall occurring during back-loaded hours, and was more concentrated in time than any of the other historical extreme events (Fig. 10a). As shown by Chen et al., (2015), short-duration, highly concentrated rainstorms tend to generate more severe flooding hazards than continuous, evenly distributed precipitation of similar magnitude.

The August 1976 event was also short (3 hours) but followed a peak-centered pattern, with rainfall occurring both before and after the peak (Fig. 10a). This event produced the second-most severe rainfall hazard in the catchment; spatially, it was more widely distributed across the catchment, with the greatest concentration near the estuarine city. Similarly, the double extreme events of 1955 (September and October) were both spatially confined to small areas: the September 1955 event was concentrated in the middle-left part of the basin, while the October 1955 event, like August 1976, was concentrated downstream to near the estuarine city but produced no rainfall in the

https://doi.org/10.5194/egusphere-2026-4780
Preprint. Discussion started: 19 August 2026

upland areas (Fig. 11a). The September 2022 event, in contrast, was concentrated upstream, more focused in the middle-right area in the basin.

These two events, September 2022 and August 1976, produced the greatest damage in the basin, driven by the combination of short temporal concentration with a spatially confined pattern (September 2022) and a broader spatial distribution combined with a locally intense peak (August 1976), as illustrated in Fig. 11a. As shown by Zhou et al. (2021), the maximum discharge in extreme precipitation events is strongly influenced by the spatial structure of precipitation, and the spatial heterogeneity of precipitation can increase flood peak magnitudes by roughly 50% on average. This confirms that the joint spatial-temporal concentration of sub-daily extreme rainfall is a key driver of greater hazard impact in a basin. The other historical extremes showed less concentrated temporal distribution but produced hazardous rainfall that resulted in flooding.

Both models' projects future 2039–2068 period of sub-daily extremes to be mostly peak-centered, with rainfall concentrated in a 3-hour window (hours 3–6), some front-loaded, and overall, more temporally concentrated than historical extremes (Fig. 10b and c). Spatially, however, these future events differ markedly from the historical ones: both models project an almost uniform spatial distribution of rainfall across the basin, with only a few exceptions showing some area-specific, spatially focused pattern comparable to the historical events (Fig. 11b and c).

https://doi.org/10.5194/egusphere-2026-4780
Preprint. Discussion started: 19 August 2026

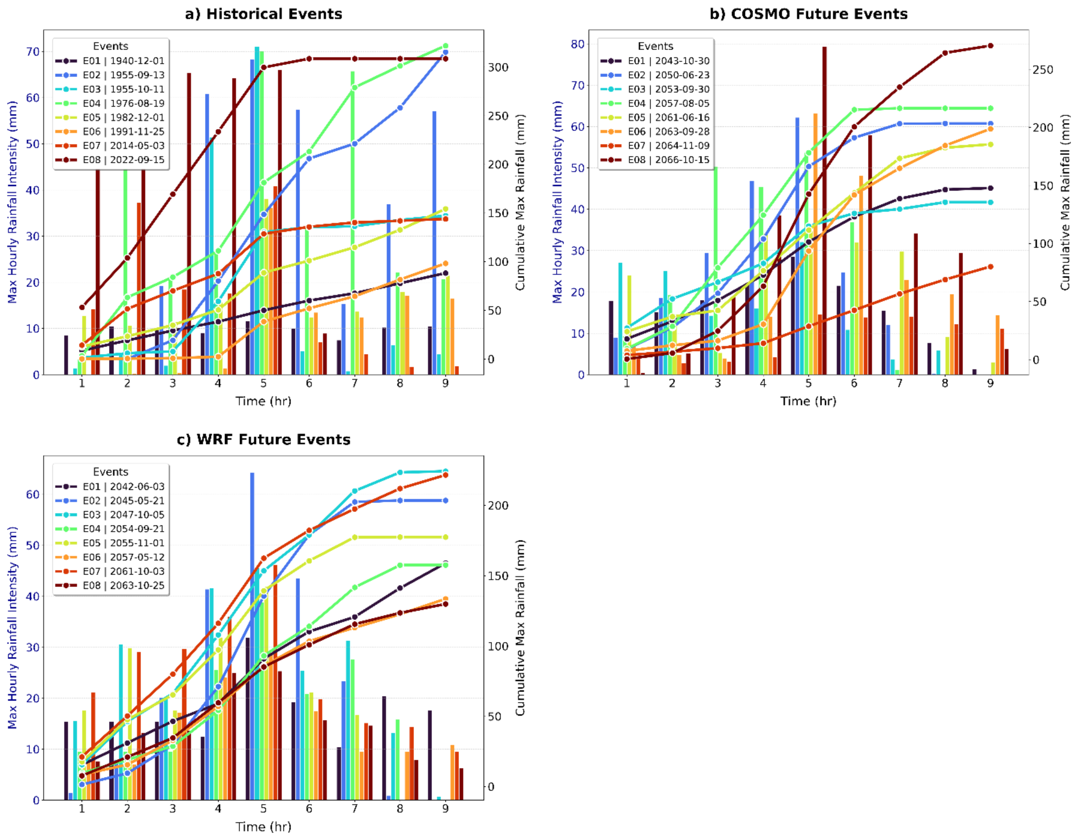

Figure 10. Hyetographs of the eight selected extreme events, labeled as from E01 to E08 for each dataset: 9-hour maximum cumulative totals and their hourly intensity for the historical extreme events **(a)**, the period of 2039–2068 future projection by the COSMO RCP8.5 **(b)** and WRF RCP8.5 **(c)** extreme events.

Table 4. Summary of the eight selected extreme precipitation events (labeled as from E01 to E08) for the three datasets used: historical events, COSMO and WRF RCP8.5 model future extreme events values of maximum and mean peak intensity, and maximum 9-hour cumulative for each dataset

Datasets	Sigle max peak intensity (mm h^{-1})	Average peak intensity of all events (mm h^{-1})	Max 9-hour cumulative of all events (mm)
Historical	71.08 (E03)	50.31	321.92 (E04)
COSMO RCP8.5	79.37 (E08)	46.10	216.52 (E08)
WRF RCP8.5	64.38 (E02)	40.39	224.25 (E03)

https://doi.org/10.5194/egusphere-2026-4780
Preprint. Discussion started: 19 August 2026

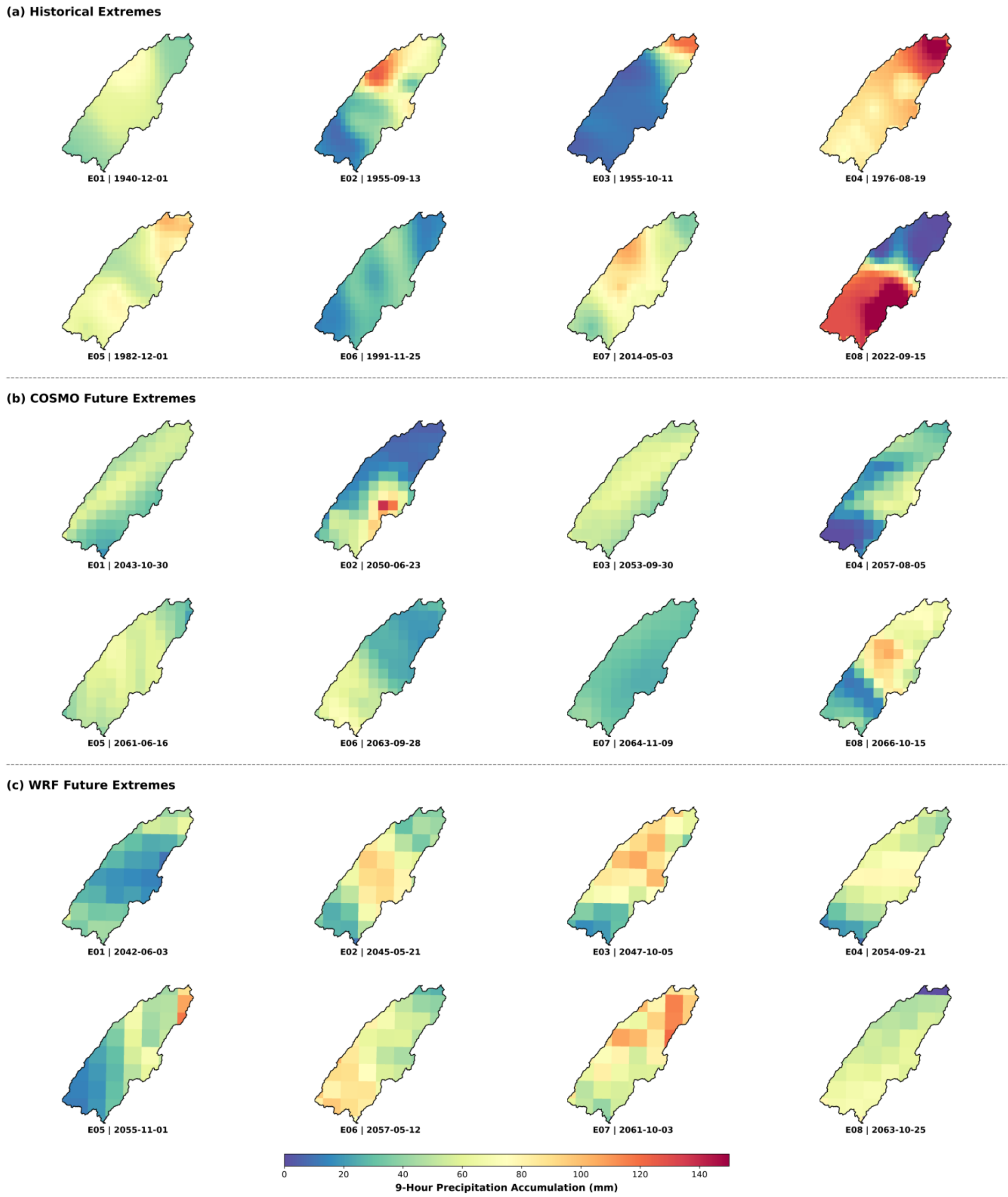

Figure 11. Spatial distribution of the 9-hour cumulative total precipitation in historical extreme events **(a)**, COSMO RCP8.5 **(b)**, and WRF RCP8.5 **(c)** projections of the 2039–2068 period of each extreme event

https://doi.org/10.5194/egusphere-2026-4780
Preprint. Discussion started: 19 August 2026

3.2.2 Magnitude and Temporal Shift of Extreme Events

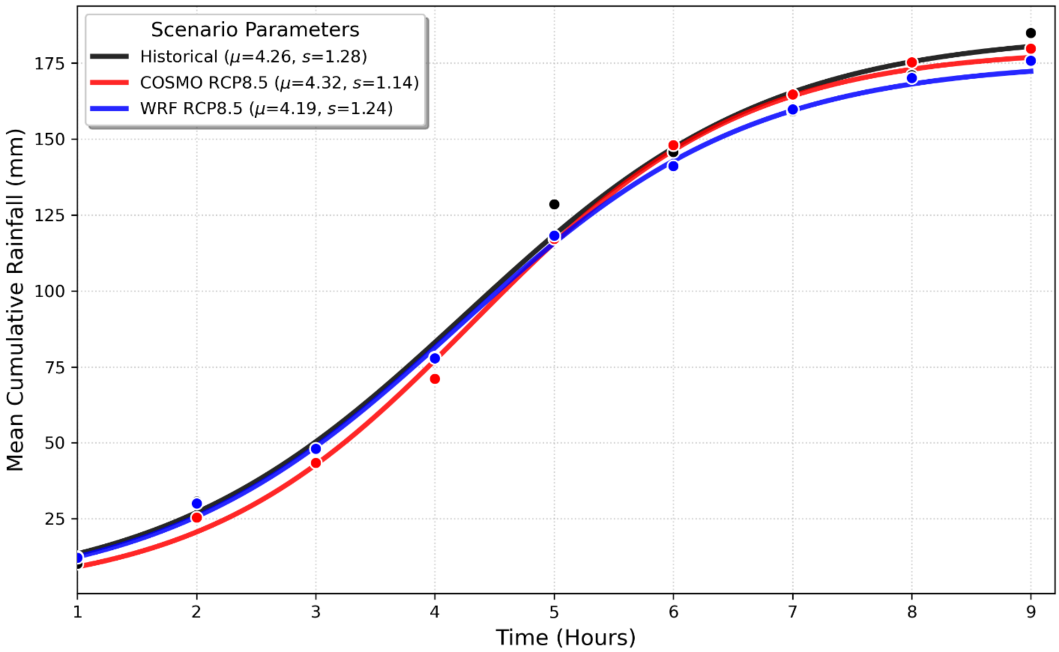

Figure 12. Mean cumulative rainfall distribution and its concentration timing (μ) and spread (s): The logistic fit graph of historical extreme events (black line) and future extreme events selected from COSMO RCP8.5 (red line) and WRF RCP8.5 (blue line) of 2039–2068 projections

Event-scale analysis of the peak-centered, normalized nine-hour mass curves characterizes the accumulation dynamics of extreme precipitation events in the Misa River basin, comparing the historical baseline with future (2039–2068) scenarios. Rather than uniform volumetric expansion over the event's duration, the results reveal a distinct structural shift under RCP8.5 (Fig. 12). Both COSMO and WRF project lower initial mass accumulations at hour 5, with negative anomalies of -8.9% (117.21 mm) and -8.1% (118.22 mm), respectively, relative to the historical value (Table 5). Accumulation rates then increase rapidly by hour 7, with future volumes temporarily matching or exceeding historical levels, 164.70 mm (+3.5%) under COSMO and 159.80 mm (+0.5%) under WRF. This may further enhance that while the early build-up phase of extreme events remains broadly similar between the historical and future periods, the largest projected changes occur near peak intensity, where rainfall becomes more concentrated in the model output. The catchment complex orography may further enhance this effect by favoring moisture uplift and local

https://doi.org/10.5194/egusphere-2026-4780
Preprint. Discussion started: 19 August 2026

intensification of precipitation (Houze, 2012). By hour 9, both model projections converge, with cumulative totals stabilizing below the historical ceiling of 184.93 mm: -2.8% for COSMO and -4.9% for WRF (Table 5 and Fig. 12).

These results are consistent with the broader literature suggesting that intensification under warming climates tends to concentrate within sub-daily, short-duration windows (Westra et al., 2014), which would imply that future extreme precipitation events could become structurally hazardous, delivering large rainfall volumes within shorter durations. However, given that this analysis relies on two regional climate models with differing resolution, driving data, and microphysical parameterizations, and on a limited, subjectively selected set of extreme events, the observed historical-to-future shift cannot be attributed to climate change alone. Differences between the two models, and between the historical and future periods, reflect a combination of model structure, resolution, forcing, physics parameterization, and event-selection effects as well as climate change (Gutowski et al., 2020), and should be interpreted as indicative rather than a definitive attribution to anthropogenic warming.

The logistic fit parameters (μ and s) provide a clear mathematical framework for quantifying these changes in dynamics. For a cumulative logistic curve, μ corresponds to the inflection point of the accumulation curve, that is, the time at which the rate of rainfall reaches its maximum, rather than the time of peak cumulative rainfall, which, by definition, occurs at the end of the event window. The location parameters (μ) remain stable across scenarios, anchored near the 4-hour mark (μ = 4.19 for WRF; μ = 4.32 for COSMO) in Fig. 12. Because the 9-hour windows are peak-centered, μ near the center is expected by construction rather than a physical signal and should not be read as an independent finding about future event timing. The more informative quantity is the scale parameter (s), which decreases from a historical value of 1.28 to 1.24 for WRF and 1.14 for COSMO under future projection. A smaller-scale parameter indicates a steeper accumulation gradient around the inflection point, consistent with a compression of rainfall into shorter, more intense sub-daily periods (Westra et al., 2014; Fowler et al., 2021). This suggests that while nine-hour cumulative totals stabilize below historical levels, the future convective core in the model projections becomes increasingly concentrated, with higher peak intensities delivered over a shorter duration around the inflection point.

https://doi.org/10.5194/egusphere-2026-4780
Preprint. Discussion started: 19 August 2026

Table 5. The future (2039–2068) extreme storm scenarios change at a specific time of the hour in a normalized nine-hour window.

Datasets	Hour 5 (Accum. /%Δ)	Hour 7 (Accum. /%Δ)	Hour 9 (Accum. /%Δ)
Historical	128.60 (Base)	159.07 (Base)	184.93 (Base)
COSMO RCP8.5	117.21 (-8.9%)	164.70 (+3.5%)	179.76 (-2.8%)
WRF RCP8.5	118.22 (-8.1%)	159.80 (+0.50%)	175.81 (-4.9%)

Moreover, the Huff curve analysis of temporal rainfall distribution complements the logistic fit results by revealing not only how extreme rainfall falls but also how it is distributed over time within an event (Huff, 1967). This non-dimensional analysis reveals a systematic reorganization of extreme-event structure between the historical and future simulations across the Misa River basin. For clarity, accumulation patterns are described here relative to the start of the 9-hour event window: front-loaded denotes disproportionate mass accumulation in the early quartiles (0–50% duration) relative to the 1:1 uniform distribution, while back-loaded denotes disproportionate accumulation in the later quartiles (50–100% duration). Under the historical baseline, extremes exhibit a front-loaded accumulation pattern, consistently exceeding the 1:1 uniform distribution line from the earliest stages; by the end of the first quartile (0–25% duration), approximately 30% of total extreme mass has already accumulated (Fig. 13).

Under the future RCP8.5 scenario (2039–2068), both models project a distinct suppression of early-stage rainfall accumulation, with curves remaining substantially below the historical profile throughout the first quartile. By the 25% duration mark, WRF has released approximately 20% of its total mass, while COSMO shows a notably reduced accumulation of approximately 10% (Fig. 13). This suppressed early accumulation sets the conditions for a more rapid rainfall release during the second and third quartiles in the model projections. Within the second quartile (25–50% duration) in Figure 13, future accumulation curves increase sharply, exhibiting rapid parallel surges in both models. WRF shows its steepest accumulation rate during this phase, crossing above the historical threshold at approximately 45% duration and reaching 60% of total extreme mass at the 50% midpoint, compared to 55% in the historical baseline.

During the third quartile (50–75% duration), COSMO shows an even more pronounced acceleration, releasing approximately half of its total storm volume within this compressed 25%-time window, while the historical baseline shows a more gradual increase from 55% to 90% across

https://doi.org/10.5194/egusphere-2026-4780
Preprint. Discussion started: 19 August 2026

the same phase. This mid-window concentration is potentially important for peak discharge generation, since storm temporal patterns loaded in the latter part of an event have been shown to substantially increase flood hazard independent of total rainfall volume (Hettiarachchi et al., 2018). The pronounced second-quartile surge in projected rainfall accumulation may promote earlier soil saturation and depression-storage filling ahead of the precipitation peak.

During the fourth quartile, future accumulation curves converge toward the uniform distribution pathway, depleting their remaining rainfall mass as they approach their final totals. This shift from early-stage accumulation suppression to concentrated mid-rainfall surges is consistent with a thermodynamic reorganization mechanism described under enhanced radiative forcing (Meredith et al., 2020; Fowler et al., 2021), though the present analysis cannot isolate that mechanism from model-structural differences, resolution effects, or the limited set of events selected for this study. The agreement between the two RCM simulations is suggestive of an elevated rainfall hazard from concentrated mid-storm intensification (Westra et al., 2014; Struglia et al., 2025); however, given differences in driving GCMs between the two models, this agreement should not be read as independent confirmation of a climate-driven signal.

For small basins such as the Misa, flood response depends on both precipitation amount and timing, in addition to other basin parameters. The projected shift toward more temporally concentrated rainfall means that a larger fraction of total precipitation mass falls within a shorter duration in the model output, even when total accumulations remain close to historical levels. The projected increase in rainfall therefore appears linked not only to stronger intensities but also to changes in the dynamical structure of extreme events; this signal cannot be fully separated from model, resolution, and forcing-related uncertainties.

https://doi.org/10.5194/egusphere-2026-4780
Preprint. Discussion started: 19 August 2026

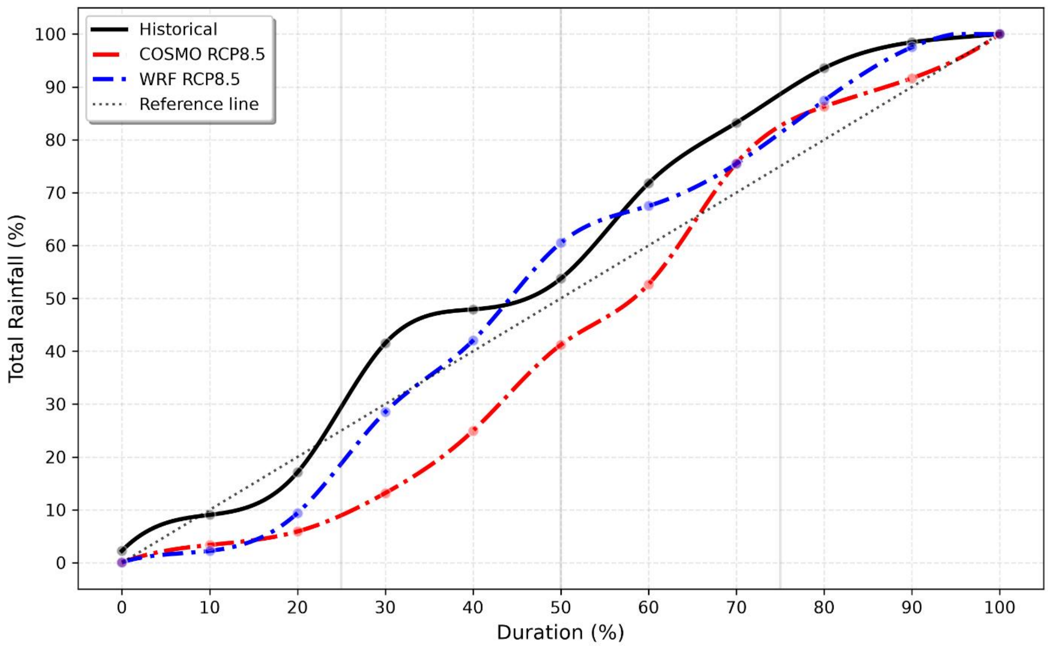

Figure 13. Huff curve graph of historical extreme events (black line) and future (2039–2068) extreme events selected from COSMO RCP8.5 (red dashed line) and WRF RCP8.5 (green dashed line) projections with a diagonal reference line (black dotted line)

3.2.3 Sensitivity analysis of sub-daily rainfall concentration

A peak-centered 9-hour temporal window captures most of the extreme intensity within an event, though not necessarily the complete event structure. Sensitivity analysis of cumulative precipitation in this 9-hour window relative to the full 24-hour window shows that, for both historical and future extremes, some events capture a core share exceeding 95% of total daily precipitation mass within a short-duration convective burst (e.g., Historical E08, COSMO E08, WRF E02), as shown in Fig. S7 in the Supplement. For these events, extreme rainfall hazard is clearly governed by an acute convective burst rather than prolonged, low-intensity accumulation. In other cases, the 9-hour core captures only 40–60% of total daily precipitation mass (e.g., Historical E06, COSMO E07, and WRF E01), reflecting either full-day rainfall of comparatively low intensity or multiple precipitation peaks occurring outside the selected window (Fig. S7 in the Supplement).

https://doi.org/10.5194/egusphere-2026-4780
Preprint. Discussion started: 19 August 2026

In these compound, multi-peak events, the single absolute hourly intensity maximum remains localized within the 9-hour core window; the window should therefore be interpreted as capturing the event's principal intensity core, not its full duration, rising limb, or recession. Secondary peaks and accumulated precipitation outside the window may still contribute meaningfully to total event volume and downstream hydrological response, even where it does not represent the single most intense hour. This general temporal concentration is broadly consistent with classic storm-profile frameworks (Huff, 1967), which describe severe convective systems as concentrating the bulk of their precipitable water within a short-duration burst. Modern temporal scaling analyses (Lengfeld et al., 2021), further support the view that 6- to 9-hour windows are well suited for capturing peak volumetric intensity and hazard potential in most extreme rainfall events, while acknowledging that a fixed-duration window will not fully represent the evolution of the event in all cases.

4. Study limitations and future perspectives

This first analysis provides insight into possible changes in extreme precipitation distribution and driving processes at the local scale but is subject to several limitations. The main limitation is the reliance on only two climate models, limiting the captured range of uncertainty. Since WRF and COSMO are driven by different GCMs (EC-Earth and CMCC-CM) under the same RCP8.5 scenario, their agreement reflects the combined influence of the driving GCM, model structure, and physics, rather than an independent confirmation of the climate signal. This study also considers only a high-emission pathway (RCP8.5); future work should include intermediate- and low-emission scenarios. Historical event hindcast, initialized event-by-event via ERA5-driven WRF, would also benefit from further sensitivity testing of spin-up length and soil-state initialization. Finally, the mass-curve and Huff-curve analyses are based on a limited event sample (8 historical and 8 future extremes per climate model), so the observed structural shifts cannot be fully separated from event-selection effects, and results should be interpreted as indicative rather than statistically exhaustive. Larger event samples, alternative threshold definitions, and broader regional climate model ensembles would help confirm the robustness of the projected shift toward more temporally concentrated extreme rainfall.

https://doi.org/10.5194/egusphere-2026-4780
Preprint. Discussion started: 19 August 2026

5. CONCLUSIONS

In this study, the two CPMs, WRF and COSMO-CLM, under RCP8.5 were used to examine historical (1979/81–2008) and future (2039–2068) basin climatology and precipitation extremes in the Misa River basin (Marche region in Italy). Quantile-based bias correction was used to reduce systematic error while preserving each model's physically coherent spatial gradients. This approach effectively realigned both models with the observed baseline, reducing COSMO's underestimation and WRF's overamplification, including a shared seasonal bias toward overestimation in spring, though residual biases remained. The results indicate a reduction in the mean annual precipitation, mainly driven by reduced future summer precipitation with July as the driest month, while mean daily precipitation in November shows an increasing signal in the future period. In contrast to these mean-state changes, extreme precipitation statistics reveal a more complex, model-dependent pattern.

The return-period analysis of both models consistently projects an intra-model increase in daily precipitation extremes relative to their own historical baselines: a historical 100-year daily event is projected to recur every 4.8 years under COSMO and 9.4 years under WRF, suggesting it could become 10 to 20 times more frequent under future climate conditions. However, when historically observed extreme magnitudes are evaluated against each model's future return-period curve, the models diverge; WRF projects reduced nearly 50%, which is a doubling of annual exceedance probability of these magnitudes, whereas COSMO shows an event-dependent response, with some becoming more frequent and others rarer. Among these, the top eight known catastrophic flood events show contrasting return-period responses depending on the model considered.

Specifically, in WRF, the observed basin maximum associated with the September 2022 event shifts from an 182-year historical return period to approximately 97 years in the future period, while the August 1976 event decreases from 94 to 47 years. Conversely, COSMO projects an increase in the estimated return periods, with the September 2022 event shifting from 182 to 860 years and the August 1976 event from 94 to 153 years. These contrasting responses highlight the uncertainty associated with future extreme precipitation projections and the sensitivity of return period estimates to the model representation of extreme events. Event-scale analysis of the top eight extreme rainfall events in a peak-centered 9-hour temporal concentration window, with peak hourly intensities diverge by +11.6% and −9.4% under COSMO and WRF, respectively, while both

https://doi.org/10.5194/egusphere-2026-4780
Preprint. Discussion started: 19 August 2026

models show a decrease in nine-hour total accumulation. Huff curve analysis indicates that these future extreme precipitation events have limited early-stage rainfall accumulation in the first quartile, then a rapid, concentrated release of precipitation in the second and third quartiles.

Overall, the results reveal that both models increase their own model-relative daily return levels, while the occurrence of the observed benchmark magnitude and the sub-daily peak responses are strongly model-dependent. These findings suggest that design standards typically based on historical climate conditions may underestimate future rainfall hazards under some projections, underscoring the need to account for model-chain uncertainty in their revision. The expected changes in rainfall intensity, frequency, and temporal concentration constitute a critical basis for future hydrological and hydraulic research. Coupling these CPM projections with distributed hydrological models would allow quantification of flood response, inundation extent, and infrastructure vulnerability across the Misa River basin.

https://doi.org/10.5194/egusphere-2026-4780
Preprint. Discussion started: 19 August 2026

Data Availability

The observation data set was downloaded from https://www.isprambiente.gov.it/it

The COSMO-CLM model data was downloaded from https://dds.cmcc.it/#/dataset/climate-projections-rcp85-downscaled-over-italy

Supplement

The supplement related to this manuscript is available in separate supplement files.

Author Contribution

All authors contributed to the preparation of this paper. DYM: conceptualization, formal analysis, methodology, writing the original draft of preparation, reviewing, and editing. MB: visualization, supervision, and reviewing. AN: conceptualization, visualization, reviewing, and editing. AP: model simulation, formal analysis, visualization, reviewing, and editing. and GL: visualization and review. The final paper was reviewed and approved by all authors.

Competing Interests

The authors declare that they have no conflict of interest.

Disclaimer

Publisher's note: Copernicus Publications remain neutral regarding jurisdictional claims made in the text, published maps, institutional affiliations, or any other geographical representation in this paper. The authors bear the ultimate responsibility for providing appropriate place names. Views expressed in the text are those of the authors and do not necessarily reflect the views of the publisher.

Acknowledgements

Authors sincerely thank the ISPRA and CMC for providing the observed and model data, respectively. Anna Napoli has been supported by “Fondazione CARITRO” (Cassa di Risparmio di Trento e Rovereto) within the project "Insight into the physical mechanisms underlying convection phenomena for a better understanding of its future evolution in the context of climate change in the Trentino region," which is acknowledged. During preparation of this manuscript, the authors used Claude (Anthropic, 2025) and Gemini (Google, 2025) to assist with language editing and improving the clarity of the sections. All content was reviewed and revised by the authors to ensure accuracy and maintain the scientific integrity of the manuscript.

Financial Support

This work is part of Mr. Meskele's PhD dissertation directly funded by UNIVPM.

REFERENCES

Aguiar, F. C., Bentz, J., Silva, J. M. N., Fonseca, A. L., Swart, R., Santos, F. D., and Penha-Lopes, G.: Adaptation to climate change at local level in Europe: An overview, Environ. Sci. Policy, 86, 38–63, https://doi.org/10.1016/j.envsci.2018.04.010, 2018.

Al-jahwari, B., Al-rawas, G., Nikoo, M. R., and Etri, T.: Robust Rainfall Gap-Filling in Coastal Arid Regions Using Ensemble Fusion Models, Hydrology, 13, 1–26, 2026.

Amir, A., David, E., Hsu, K., Schubert, S., and Sorooshian, S.: Extremes in a Changing Climate: Detection, Analysis and Uncertainty, Springer Dordrecht, 426 pp., https://doi.org/10.1007/978-94-007-4479-0, 2013.

Apicella, L., Puca, S., Lagasio, M., Meroni, A. N., Milelli, M., Vela, N., Garbero, V., Ferraris, L., and Parodi, A.: The predictive capacity of the high resolution weather research and forecasting model : a year-long verification over Italy, Bull. Atmos. Sci. Technol., 2, 2021.

Ban, N., Schmidli, J., and Schär, C.: Evaluation of the convection-resolving regional climate modeling approach in decade-long simulations, J. Geophys. Res., 119, 7889–7907, https://doi.org/10.1002/2014JD021478., 2014.

Ban, N., Rajczak, J., Schmidli, J., and Schär, C.: Analysis of Alpine precipitation extremes using generalized extreme value theory in convection-resolving climate simulations, Clim. Dyn., 55, 61–75, https://doi.org/10.1007/s00382-018-4339-4, 2020.

Bangelesa, F., Merkenschlager, C., Hertig, E., and Paeth, H.: Improved bioclimatic variables from regional climate models : a comparative analysis of three classic bias adjustment methods and a novel adjustment approach, Theor. Appl. Climatol., 157, 2026.

Bannister, D., Orr, A., Jain, S. K., Holman, I. P., and Momblanch, A.: Bias Correction of High - Resolution Regional Climate Model Precipitation Output Gives the Best Estimates of Precipitation in Himalayan Catchments Journal of Geophysical Research : Atmospheres, J. Geophys. Res., 124, 14220–14239, https://doi.org/10.1029/2019JD030804, 2019.

Berg, P., Christensen, O. B., Klehmet, K., Lenderink, G., Olsson, J., Teichmann, C., and Yang, W.: Summertime precipitation extremes in a EURO-CORDEX 0.11 degree ensemble at an hourly resolution, Nat. Hazards Earth Syst. Sci., 19, 957–971, https://doi.org/10.5194/nhess-19-957-2019, 2019.

Berthou, S., Kendon, E. J., Chan, S. C., Ban, N., Leutwyler, D., Schär, C., and Fosser, G.: Pan-European climate at convection-permitting scale: a model intercomparison study, Clim. Dyn., 55, 35–59, https://doi.org/10.1007/s00382-018-4114-6, 2020.

Blöschl, G., Hall, J., Viglione, A., Perdigão, R. A. P., Parajka, J., Merz, B., Lun, D., Arheimer, B., Aronica, G. T., Bilibashi, A., Boháč, M., Bonacci, O., Borga, M., Čanjevac, I., Castellarin, A., Chirico, G. B., Claps, P., Frolova, N., Ganora, D., Gorbachova, L., Gül, A., Hannaford, J., Harrigan, S., Kireeva, M., Kiss, A., Kjeldsen, T. R., Kohnová,

https://doi.org/10.5194/egusphere-2026-4780
Preprint. Discussion started: 19 August 2026

S., Koskela, J. J., Ledvinka, O., Macdonald, N., Mavrova-Guirguinova, M., Mediero, L., Merz, R., Molnar, P., Montanari, A., Murphy, C., Osuch, M., Ovcharuk, V., Radevski, I., Salinas, J. L., Sauquet, E., Šraj, M., Szolgay, J., Volpi, E., Wilson, D., Zaimi, K., and Živković, N.: Changing climate both increases and decreases European river floods, Nature, 573, 108–111, https://doi.org/10.1038/s41586-019-1495-6, 2019.

Bonta, J. V: Development And Utility of Huff Curves for Disaggregating Precipitation Amounts, Appl. Eng. Agric., 20, 641–656, 2004.

Brocchini, M., Postacchini, M., Lorenzoni, C., Russo, A., Corvaro, S., Mancinelli, A., Soldini, L., Calantoni, J., Reed, A. H., Braithwaite, E. F., Sheremet, A., Staples, T., and Smith, J.: Comparison between the wintertime and summertime dynamics of the Misa River estuary, Mar. Geol., 385, 27–40, https://doi.org/10.1016/j.margeo.2016.12.005, 2017.

Brunetti, M., Maugeri, M., Monti, F., and Nanni, T.: Temperature and Precipitation Variability in Italy in the Last Two Centuries from Homogenized Instrumental Time, Int. J. Climatol., 26, 345–381, https://doi.org/10.1002/joc.1251, 2006.

Brunner, M., Clark, M., Gilleland, E., Wood, A., and Swain, D. L.: Spatial Dependence of Floods Shaped by Spatiotemporal Variations in Meteorological and Land - Surface Processes Geophysical Research Letters, Geophys. Res. Lett., 47, 1–13, https://doi.org/10.1029/2020GL088000, 2020.

Bucchignani, E., Montesarchio, M., and Zollo, L.: High-resolution climate simulations with COSMO-CLM over Italy : performance evaluation and climate projections for the 21st century, Int. J. Climatol., 36, 735–756, https://doi.org/10.1002/joc.4379, 2016.

Cannon, A. J., Sobie, S. R., and Murdock, T. Q.: Bias Correction of GCM Precipitation by Quantile Mapping : How Well Do Methods Preserve Changes in Quantiles and Extremes ?, J. Clim., 28, 6938–6959, https://doi.org/10.1175/JCLI-D-14-00754.1, 2015.

Cardoso, R. M., Soares, P. M. M., Miranda, P. M. A., and Belo-pereira, M.: WRF high resolution simulation of Iberian mean and extreme precipitation climate, Int. J. Climatol., https://doi.org/10.1002/joc.3616, 2012.

Chang, Y. and Burningham, H.: Gap Filling of Daily Weather Data using Spatial Interpolation Techniques and Neural Network Methods, J. Coast. Res., 113, 463, https://doi.org/10.2112/JCR-SI113-091.1, 2024.

Chen, Z., Yin, L., Chen, X., and Zhu, Z.: Research on the characteristics of urban rainstorm pattern in the humid area of Southern China : a case study of Guangzhou city, Int. J. Climatol., 4386, 4370–4386, https://doi.org/10.1002/joc.4294, 2015.

Coles, S.: An Introduction to Statistical Modeling of Extreme Values, 209 pp., https://doi.org/10.1007/978-1-4471-3675-0, 2001.

Corti, M., Francioni, M., Abbate, A., Papini, M., and Longoni, L.: Analysis and Modelling of the September 2022 Flooding Event in the Misa Basin, Ital. J. Eng. Geol. Environ., 1, 69–76, https://doi.org/10.4408/IJEGE.2024-01.S-08, 2024.

Dahm, R., Bhardwaj, A., Weiland, F. S., Corzo, G., and Bouwer, L. M.: A Temperature-Scaling Approach for Projecting Changes in Short Duration Rainfall Extremes from GCM Data, Water, 11, 1–15, https://doi.org/10.3390/w11020313, 2019.

Dallan, E., Marra, F., Borga, M., and Zaramella, M.: Enhanced Summer Convection Explains Observed Trends in Extreme Subdaily Precipitation in the Eastern Italian Alps Geophysical Research Letters, Geophys. Res. Lett., 49, https://doi.org/10.1029/2021GL096727, 2022.

Dallan, E., Marra, F., Fosser, G., Marani, M., and Borga, M.: Dynamical Factors Heavily Modulate the Future Increase of Sub - Daily Extreme Precipitation in the Alpine - Mediterranean Region Earth ' s Future, Earth's Futur., 12, 1–16, https://doi.org/10.1029/2024EF005185, 2024.

Derdour, S., Ghenim, A. N., Megnounif, A., and Tangang, F.: Bias Correction and Evaluation of Precipitation Data from the CORDEX Regional Climate Model for Monitoring Climate Change in the Wadi Chemora Basin (Northeastern Algeria), Atmosphere (Basel)., 13, 1876, 2022.

Donnini, M., Santangelo, M., Gariano, S. L., Bucci, F., Peruccacci, S., Alvioli, M., Althuwaynee, O., Ardizzone, F., Bianchi, C., Bornaetxea, T., Brunetti, M. T., Cardinali, M., Esposito, G., Grita, S., Marchesini, I., Melillo, M., Salvati, P., Yazdani, M., and Fiorucci, F.: Landslides triggered by an extraordinary rainfall event in Central Italy on September

15, 2022, Landslides, 20, 2199–2211, https://doi.org/10.1007/s10346-023-02109-4, 2023.

Faggian, P.: Future Precipitation Scenarios over Italy, Water, 13, 1335, 2021.

Feser, F. and Shepherd, T. G.: The concept of spectrally nudged storylines for extreme event attribution, J. Commun. earth Environ., 6, 1–8, 2025.

Findell, K. and Elfatih, E.: Atmospheric Controls on Soil Moisture – Boundary Layer Interactions . Part I : Framework Development, J. Hydrometeorol., 4, 552–569, 2003.

Fosser, G., Khodayar, S., and Berg, P.: Benefit of convection permitting climate model simulations in the representation of convective precipitation, Clim. Dyn., 44, 45–60, https://doi.org/10.1007/s00382-014-2242-1, 2015.

Fowler, H. J., Lenderink, G., Prein, A. F., Westra, S., Allan, R. P., Ban, N., Barbero, R., Berg, P., Blenkinsop, S., Do, H. X., Guerreiro, S., Haerter, J. O., Kendon, E. J., Lewis, E., Schaer, C., Sharma, A., Villarini, G., Wasko, C., and Zhang, X.: Anthropogenic intensification of short-duration rainfall extremes, Nat. Rev. Earth Environ., 2, 107–122, https://doi.org/10.1038/s43017-020-00128-6, 2021.

Gentilucci, M., Rossi, A., Pelagagge, N., Aringoli, D., Barbieri, M., and Pambianchi, G.: GEV Analysis of Extreme Rainfall : Comparing Different Time Intervals to Analyse Model Response in Terms of Return Levels in the Study Area of Central Italy, Sustainability, 15, 11656, 2023.

Giuseppe, S. and Rossano, M.: Piogge Intense, Inondazioni e Alluvioni Storiche a Senihallia, Parte Seco., Biblioteca Comunale Antonelliana Senigallia 2021, 198 pp., 2021.

Gringorten, I. I.: A plotting rule for extreme probability paper, J. Geophys. Res., 68, 813–814, https://doi.org/10.1029/JZ068i003p00813, 1963.

Gutowski, J. W. J., Ullrich, P. A., Hall, A., Leung, L. R., O'Brien, T. A., Patricola-DiRosario, C. M., Arritt, R. W., Bukovsky, M. S., Calvin, K. V, Feng, Z., Jones, A. D., and Kooperman, G. J.: The Ongoing Need for High-Resolution Regional Climate Models, Bull. Am. Meteorol. Soc., 664–683, 2020.

Haerter, J. O., Hagemann, S., Moseley, C., and Piani, C.: Climate model bias correction and the role of timescales, Hydrol. Earth Syst. Sci., 15, 1065–1079, https://doi.org/10.5194/hess-15-1065-2011, 2011.

Hagos, S. M., Ruby, L., Oluwayemi A., G., Charlotte, D., Bryce, H., Jian, L., and Min-Seop, A.: The Relationship between Precipitation and Precipitable Water in CMIP6 Simulations and Implications for Tropical Climatology and Change, J. Clim., 34, 1587–1600, https://doi.org/10.1175/JCLI-D-20-0211.1, 2021.

Han, J. and Pan, H.-L.: Revision of Convection and Vertical Diffusion Schemes in the NCEP Global Forecast System, Weather Forecast, 26, 520–533, https://doi.org/10.1175/WAF-D-10-05038.1, 2011.

Held, I. M. and Soden, B. J.: Robust Responses of the Hydrological Cycle to Global Warming, J. Clim., 19, 5686–5699, 2006.

Hettiarachchi, S., Wasko, C., and Sharma, A.: Increase in flood risk resulting from climate change in a developed urban watershed – the role of storm temporal patterns, Hydrol. Earth Syst. Sci., 22, 2041–2056, 2018.

Hong, S.-Y., Noh, Y., and Dudhia, J.: A New Vertical Diffusion Package with an Explicit Treatment of Entrainment Processes, Mon. Weather Rev., 134, 2318, https://doi.org/10.1175/MWR3199.1, 2006.

Houze, J. R. A.: Orographic effects on precipitating clouds, Rev. Geophys., 50, https://doi.org/10.1029/2011RG000365, 2012.

Huff, F. A.: Time Distribution Rainall in Heavy Storms be used in hydrologic design proble ms or, Water Resour. Res., 3, 1007–1019, 1967.

Iacono, M. J., Delamere, J. S., Mlawer, E. J., Shephard, M. W., Clough, S. A., and Collins, W. D.: Radiative forcing by long-lived greenhouse gases: Calculations with the AER radiative transfer models, J. Geophys. Res., 113, D13103, https://doi.org/10.1029/2008JD009944, 2008.

IPCC: Climate Change 2023: Synthesis Report, 1–42 pp., 2023.

Ivanov, M. A., Luterbacher, J., and Kotlarski, S.: Climate Model Biases and Modification of the Climate Change Signal by Intensity-Dependent Bias Correction, J. Clim., 31, 6591–6610, https://doi.org/10.1175/JCLI-D-17-0765.1, 2018.

Kao, S. C. and Ganguly, A. R.: Intensity , duration , and frequency of precipitation extremes under 21st - century

https://doi.org/10.5194/egusphere-2026-4780
Preprint. Discussion started: 19 August 2026

warming scenarios, J. Geophys. Res., 116, 1–14, https://doi.org/10.1029/2010JD015529, 2011.

Kendon, E. J., Prein, A. F., Senior, C. A., Stirling, A., Office, M., and Centre, H.: Challenges and outlook for convection-permitting climate modelling, Philos. Trans. R. Soc. A, 379, https://doi.org/10.1098/rsta.2019.0547, 2021.

Kendon, J. E., Nigel, M. R., Catherine, A. S., and Malcolm, J. R.: Realism of Rainfall in a Very High-Resolution Regional Climate Model, J. Clim., 25, 5791–5806, https://doi.org/10.1175/JCLI-D-11-00562.1, 2012.

Koutsoyiannis, D. and Foufoula-Georgiou, E.: A Scaling Model of a Storm Hyetograph, Water Resour. Res., 29, 2345–2361, 1993.

Ledda, A., Anna, E., Cesare, D., Satta, G., Cocco, G., Calia, G., Arras, F., Congiu, A., Manca, E., and Montis, A. De: Adaptation to Climate Change and Regional Planning : A Scrutiny of Sectoral Instruments, Sustainability, 12, 1–15, 2020.

Lengfeld, K., Walawender, E., Winterrath, T., Becker, A., Wetterdienst, D., Straße, F., and Main, O.: CatRaRE : A Catalogue of radar-based heavy rainfall events in Germany derived from 20 years of data, Meteorol. Zeitschrift (Contributions to Atmos. Sci., 30, 469–487, https://doi.org/10.1127/metz/2021/1088, 2021.

Li, R. L., Studholme, J. H. P., Fedorov, A. V, and Storelvmo, T.: Increasing Precipitation Efficiency Amplifies Climate Sensitivity by Enhancing Tropical Circulation Slowdown and Eastern Pacific Warming Pattern, Geophys. Res. Lett., 50, https://doi.org/10.1029/2022GL100836, 2023.

Lu, G. Y. and Wong, D. W.: Computers & Geosciences An adaptive inverse-distance weighting spatial interpolation technique, Comput. Geosci., 34, 1044–1055, https://doi.org/10.1016/j.cageo.2007.07.010, 2008.

Lucas-Picher, P., Argüeso, D., Tramblay, Y., Berg, P., and Lemonsu, A.: Convection-permitting modeling with regional climate models : Latest developments and next steps, WIREs Clim. Chang., 12, 1–59, https://doi.org/10.1002/wcc.731, 2021.

Maines, E., Crespi, A., Pittore, M., and Zebisch, M.: Recent and future variability in 1-day precipitation extremes in Trentino – South Tyrol (Eastern Italian Alps) based on observations (1956-2023) and climate model projections, Weather Clim. Extrem., 52, 100880, https://doi.org/10.1016/j.wace.2026.100880, 2026.

Manabe, S. and Wetherald, R.: Large-scale changes of soil wetness induced by an increase in atmospheric carbon dioxide, J. Atmos. Sci., 44, 1211–1236, 1987.

Maraun, D.: Bias Correction , Quantile Mapping , and Downscaling : Revisiting the Inflation Issue, J. Clim., 26, 2137–2143, https://doi.org/10.1175/JCLI-D-12-00821.1, 2013.

Marco, I., Matteo, P., Giovanna, D., and Perugini, E.: Hydrodynamic Modeling of the Final Reach of the Misa River (Senigallia, Italy): The Role of Sea Action and Bed Forms, 1–107 pp., 2021.

Mattavelli, R.: Analysis of the erosional processes following the September 2022 flood in the Misa basin, MSc Thesis, University of Polytechnic Milano, Italy, 1–150 pp., 2023.

Menapace, A., Dhawan, P., Dalla Torre, D., Kaffas, K., Crespi, A., Larcher, M., Righetti, M., and Cannon, A. J.: Review of bias correction methods for climate model outputs in hydrology, J. Hydrol., 660, 133213, https://doi.org/10.1016/j.jhydrol.2025.133213, 2025.

Mendez, M., Calvo-Valverde, L.-A., Hidalgo-Madriz, J.-A., and Araya-Obando, J.-A.: Assessing the Effect of Bias Correction Methods on the Development of Intensity–Duration–Frequency Curves Based on Projections from the CORDEX Central America GCM-RCM Multimodel-Ensemble, Water, 16, https://doi.org/10.3390/w16233473, 2024.

Meredith, E. P., Ulbrich, U., and Rust, H. W.: Subhourly rainfall in a convection-permitting model, Environ. Res. Lett., 15, 34031, https://doi.org/10.1088/1748-9326/ab6787, 2020.

Myhre, G., Alterskjær, K., Stjern, C. W., Hodnebrog, Ø., Marelle, L., Sillmann, J., Schaller, N., Fischer, E., Schulz, M., and Stohl, A.: Frequency of extreme precipitation increases extensively with event rareness under global warming, https://doi.org/10.1038/s41598-019-52277-4, 2019.

Napoli, A., Antonio, P., Jost von, H., and Pasquero, C.: Altitudinal dependence of projected changes in occurrence of extreme events in the Great Alpine Region, Int. J. Climatol., 43, 5813–5829, https://doi.org/10.1002/joc.8222, 2023.

Nguyen, C., Vaze, J., Mateo, C. M. R., Hutchinson, M. F., and Teng, J.: Very high spatial and temporal resolution rainfall data for accurate flood inundation modelling, Hydrol. Earth Syst. Sci., 1–31, 2024.

https://doi.org/10.5194/egusphere-2026-4780
Preprint. Discussion started: 19 August 2026

Overeem, A., Buishand, A., and Holleman, I.: Rainfall depth-duration-frequency curves and their uncertainties, J. Hydrol., 348, 124–134, https://doi.org/10.1016/j.jhydrol.2007.09.044, 2008.

Papalexiou, S. M. and Koutsoyiannis, D.: Battle of extreme value distributions: A global survey on extreme daily rainfall, Water Resour. Res., 49, 187–201, https://doi.org/10.1029/2012WR012557, 2013.

Pichelli, E., Coppola, E., Sobolowski, S., Ban, N., Giorgi, F., and Stocchi, P.: The first multi - model ensemble of regional climate simulations at kilometer - scale resolution part 2 : historical and future simulations of precipitation, Clim. Dyn., https://doi.org/10.1007/s00382-021-05657-4, 2021.

Pieri, A. B., Hardenberg, J. Von, Parodi, A., and Provenzale, A.: Sensitivity of Precipitation Statistics to Resolution , Microphysics , and Convective Parameterization : A Case Study with the High-Resolution WRF Climate Model over Europe, J. Hydrometeorol., 16, 1857–1872, https://doi.org/10.1175/JHM-D-14-0221.1, 2015.

Portuguez-maurtua, M., Arumi, L., Lagos, O., Stehr, A., and Arquiñigo, N. M.: Filling Gaps in Daily Precipitation Series Using Regression and Machine Learning in Inter-Andean Watersheds, Water, 14, 1799, 2022.

Prein, A. F., Langhans, W., Fosser, G., Ferrone, A., Ban, N., Keller, M., Tölle, M., Gutjahr, O., Feser, F., and Brisson, E.: A review on regional convection-permitting climate modeling : Demonstrations , prospects , and challenges, Rev. Geophys., 53, 323–361, https://doi.org/10.1002/2014RG000475.Received, 2015.

Prein, A. F., Rasmussen, R. M., Ikeda, K., Liu, C., Clark, M. P., and Holland, G. J.: The future intensification of hourly precipitation extremes, Nat. Clim. Chang., 7, 48–52, https://doi.org/10.1038/nclimate3168, 2017.

Raffa, M., Adinolfi, M., Reder, A., Marras, G. F., Marco, M., Scipione, G., Santini, M., and Mercogliano, P.: Very High Resolution Projections over Italy under different CMIP5 IPCC scenarios, 1–13 pp., https://doi.org/10.1038/s41597-023-02144-9, 2023.

Rajczak, J. and Schär, C.: Projections of future precipitation extremes over Europe: A multimodel assessment of climate simulations, J. Geophys. Res. Atmos., 122, `10773-10799, https://doi.org/10.1002/2017JD027176, 2017.

Rockel, B., Will, A., and Hense, A.: The Regional Climate Model COSMO-CLM (CCLM), Meteorol. Zeitschrift, 17, 347–348, https://doi.org/10.1127/0941-2948/2008/0309, 2008.

Salas, J. D., Asce, M., Obeysekera, J., and Asce, M.: Revisiting the Concepts of Return Period and Risk for Nonstationary Hydrologic Extreme Events, J. Hydrol. Eng., 554–568, https://doi.org/10.1061/(ASCE)HE.1943-5584.0000820., 2014.

Serrano-notivoli, R., Beguería, S., Saz, M. Á., and Longares, L. A.: SPREAD : a high-resolution daily gridded precipitation dataset for Spain – an extreme events frequency and intensity overview, Earth Syst. Sci. data, 9, 721–738, 2017.

Shabestanipour, G., Brodeur, Z., Manoli, B., Birnbaum, A., Steinschneider, S., and Lamontagne, J. R.: Risk-based hydrologic design under climate change using stochastic weather and watershed modeling, Front. Water, Volume 6-2024, https://doi.org/10.3389/frwa.2024.1310590, 2024.

Sharif, R. B., Maggioni, V., and Dollan, I. J.: Changes in historical and future precipitation patterns across the contiguous United States, Front. Earth Sci., 13, https://doi.org/10.3389/feart.2025.1542536, 2025.

Shepherd, T. G., Boyd, E., Calel, R. A., Chapman, S. C., Dessai, S., Dima-west, I. M., Fowler, H. J., and James, R.: Storylines : an alternative approach to representing uncertainty in physical aspects of climate change, Clim. Chang., 151, 555–571, 2018.

Smirnova, T. G., Brown, J. M., and Benjamin, S. G.: Performance of Different Soil Model Configurations in Simulating Ground Surface Temperature and Surface Fluxes, Mon. Weather Rev., 125, 1870–1884, 1996.

Smirnova, T. G., Brown, J. M., Benjamin, S. G., and Kim, D.: Parameterization of cold-season processes in the MAPS land-surface scheme, J. Geophys. Res., 105, 4077–4086, 2000.

Struglia, M. V., Anav, A., Antonelli, M., Calmanti, S., Catalano, F., Aquila, A. D., Pichelli, E., Pisacane, G., Maria, C., and Struglia, V.: Impact of spatial resolution on multi-scenario WRF-ARW simulations driven by the CMIP6 MPI-ESM1-2-HR global model : a focus on precipitation distribution over Italy, Geosci. Model Dev., 18, 6095–6116, 2025.

Sun, Y., Solomon, S., Dai, A., and Portmann, R. W.: How Often Does It Rain?, J. Clim., 19, 916–934, https://doi.org/10.1175/JCLI3672.1, 2006.

Tartaglione, N.: Unprecedented Flooding in the Marche Region (Italy): Analyzing the 15 September 2022 Event and

https://doi.org/10.5194/egusphere-2026-4780
Preprint. Discussion started: 19 August 2026

Its Unique Meteorological Conditions, Meteorology, 4, 3, https://doi.org/10.3390/meteorology4010003, 2025.

Teegavarapu, R. S. V and Chandramouli, V.: Improved weighting methods , deterministic and stochastic data-driven models for estimation of missing precipitation records, J. Hydrol., 312, 191–206, https://doi.org/10.1016/j.jhydrol.2005.02.015, 2005.

Teutschbein, C. and Seibert, J.: Bias correction of regional climate model simulations for hydrological climate-change impact studies: Review and evaluation of different methods, J. Hydrol., 456–457, 12–29, https://doi.org/10.1016/j.jhydrol.2012.05.052, 2012.

Thompson, G. and Eidhammer, T.: A Study of Aerosol Impacts on Clouds and Precipitation Development in a Large Winter Cyclone, J. Atmos. Sci., 71, 3636–3658, https://doi.org/10.1175/JAS-D-13-0305.1, 2014.

Thompson, G., Field, P. R., Rasmussen, R. M., and Hall, W. D.: Explicit Forecasts of Winter Precipitation Using an Improved Bulk Microphysics Scheme . Part II : Implementation of a New Snow Parameterization, Mon. Weather Rev., 136, 5095–5115, https://doi.org/10.1175/2008MWR2387.1, 2008.

Tiedtke, M.: A Comprehensive Mass Flux Scheme for Cumulus Parameterization in Large-Scale Models, Mon. Weather Rev., 117, 1779, https://doi.org/10.1175/1520-0493(1989)117<1779:ACMFSF>2.0.CO;2, 1989.

Torma, C., Giorgi, F., and Coppola, E.: Added value of regional climate modeling over areas characterized by complex terrain-Precipitation over the Alps, J. Geophys. Res. Atmos., 120, 3957–3972, https://doi.org/10.1002/2014JD022781, 2015.

Trenberth, K. E., Dai, A., Rasmussen, R. M., and Parsons, D. B.: The changing character of precipitation, Am. Meteorol. Soc., 205–218, 2003.

Verol, A. P., Lourenço, I. B., Fraga, R., Battemarco, B. P., Merlo, M. L., Canedo, P., and Magalh, D.: River Restoration Integrated with Sustainable Urban Water Management for Resilient Cities, Sustainability, 12, 4677, 2020.

Virtanen, P., Gommers, R., Oliphant, T. E., Haberland, M., Reddy, T., Walt, S. J. Van Der, Brett, M., Wilson, J., and Millman, K. J.: SciPy 1.0: fundamental algorithms for scientific computing in Python, Nat. Methods, 17, 261–275, https://doi.org/10.1038/s41592-019-0686-2, 2020.

Volpi, E., Fiori, A., Grimaldi, S., Lombardo, F., and Koutsoyiannis, D.: One hundred years of return period: Strengths and limitations, Water Resour. Res., 51, 8570–8585, https://doi.org/10.1002/2015WR017820.Received, 2015.

Westra, S., Mehrotra, R., Sharma, A., and Srikanthan, R.: Continuous rainfall simulation : 1 . A regionalized subdaily disaggregation approach, Water Resour. Res., 48, 1–16, https://doi.org/10.1029/2011WR010489, 2012.

Westra, S., Fowler, H. J., Evans, J. P., Alexander, L. V., Berg, P., Johnson, F., Kendon, E. J., Lenderink, G., and Roberts, N. M.: Future changes to the intensity and frequency of short-duration extreme rainfall, Rev. Geophys., 52, 522–555, https://doi.org/10.1002/2014RG000464.Received, 2014.

Zambrano, V. H., Martínez, L. S., Pontón, A. H., and Ramirez-avila, J. J.: Regionalization of Short-Duration Storm Temporal Patterns Using Huff Curves in a Coastal Tropical Region, Hydrology, 13, 1–17, 2026.

Zhou, Z., Smith, J. A., Baeck, M. L., Wright, D. B., Smith, B. K., and Liu, S.: The impact of the spatiotemporal structure of rainfall on flood frequency over a small urban watershed : an approach coupling stochastic storm transposition and hydrologic modeling, Hydrol. Earth Syst. Sci., 25, 4701–4717, 2021.